Design, analysis, and optimization of photonic crystal Sensors

Mohammad Javad Safdari

A Thesis

in

The Department

of

Electrical and Computer Engineering

Presented in Partial Fulfillment of the Requirements

For the Degree of Master of Applied Science at

Concordia University

Montreal, Quebec, Canada

June 2018

CONCORDIA UNIVERSITY

SCHOOL OF GRADUATE STUDIES

This is to certify that the thesis prepared

By: Mohammad Javad Safdari

Entitled: Design, analysis, and optimization of photonic crystal Sensors

and submitted in partial fulfillment of the requirements for the degree of

Master of Applied Science

Complies with the regulations of this University and meets the accepted standards with respect to originality and quality.

Signed by the final Examining Committee:

____ Chair

Dr. D. Qiu

____ Examiner

Dr. C. Grova(Physics)

____ Examiner

Dr. Y. Shayan

____ Supervisor

Dr. J. X. Zhang

____ Supervisor

Dr. P. Bianucci

Approved by ____

Dr. W. E. Lynch, Chair

Department of Electrical and Computer Engineering

______________ 20___ ___________________________________

Dr. Amir Asif, Dean

Faculty of Engineering and Computer Science

ABSTRACT

Design, analysis, and optimization of photonic crystal Sensors

Mohammad Javad Safdari

It has been more than 30 years that Photonic Crystal (PhC) have been used in wide variety of applications. The photonic bandgap phenomenon and the flexibility of such structures to manipulate the light have made them popular. PhC sensors are popular because of their promising characteristics like high measurement sensitivity, ultra-compact size, suitability for monolithic integration, and flexibility in structural design. In this thesis, a novel framework for designing optimized PhC sensors has been proposed. The complexity of such structures resulted in the lack of an analytical method to design the structures. Therefore, this framework aims to provide a comprehensive and automatic method to find the best values for the structural parameters without human involvement. The framework is explained with an example of designing a PhC liquid sensor. In the framework, an optimizer called Multi-Objective Gray Wolf Optimizer is utilized. However, a diverse range of multi-objective optimizer algorithms could be utilized. The results show that the proposed framework can design any kind of PhC sensor. Simplicity, being straightforward, and no human involvement are the advantages of the proposed framework. In addition, a significantly wide range of optimal designs will be found which are suitable for general and specific applications.

Acknowledgement

First of all, I must pay my sincere gratitude to my supervisors Dr. (John) Xiupu Zhang and Dr. Pablo Bianucci for their support and insightful comments during the thesis duration.

Furthermore, I would like to appreciate my groupmates in both Engineering and Physics department, especially Mr. Seyedmohammad Mirjalili and Dr. Hakim Mellah. I have learned many things from them.

I would like to thank Sumaiya Gangat and his team in Concordia University Student Parent Center (CUSP) as they have supported me during this time.

I would also like to thank Dr. Saeed Azad for reviewing and helping me to complete my thesis.

At the end, I would also like to thank my spouse, Arezoo Roohi, who always provided me with an ideal condition for passing this stage of my education successfully and also my little son Liam who makes our family bigger and happier.

Table of Contents

List of Figures

List of tables

Chapter 1 Photonic Crystal

1-1 Introduction

Since photonic crystals (PhC, dielectric structures with an alternative change in refractive index) show an interesting behavior when they interact with light, similar to the electrons in semiconductors, they have been recently attracted more attention. In fact, this similarity is due to the similarity of Schrödinger equation in solid state physics and Helmholtz in electromagnetism in which behavior of the refractive index of the later is similar to that of the electrical potential in the one. Therefore, the performance of PhC (alternative refractive index structures) against photons is similar to that of the semiconductor crystals (structures with alternative electrical potentials) against electrons.

To propagate the electromagnetic wave, there must be a correspondence between the emission wavelength and the dimensions of the PhC. It is possible to use photonic crystals with a millimeter and micrometer dimensions to control microwave and infrared waves, respectively. The propagation of the waves in an environment is described with the dispersion relation between frequency and wave vector. However, the dispersion relation with respect to a non-homogeneous material can be quite complex. The propagation of waves in a crystal will generally depend on direction of the wave entry to the crystal. The most important effect of creating a band structure for PhCs is periodicity. The wavelengths of light that are allowed to propagate are called mode and allowed propagated modes form the energy bands. However, there are continuous and bounded ranges of frequency within the band structure which don't allow the propagation of the wave in PhCs as called photonic gaps.

The width and depth of the gap are characterized by the size and periodicity of the crystal lattice geometry. Due to the symmetry, crystals in certain directions have gap. The band gap can be determined theoretically and experimentally for two- and three-dimensional PhCs.

In the context of PhCs, various factors such as density, polarization, defects, etc., should be considered to control the band. When the transitional symmetry of the periodic lattice is destroyed due to a defect in the crystal lattice, the regular periodic structure of the PhCs is changed and a defect in the crystal is formed. The defect in PhCs can be caused by a change in the dielectric constant, the thickness of a layer, and so on. Defects in PhCs are similar to impurities in semiconductors. Introducing the impurities in the semiconductor, energy levels are created in the energy band. The type and size of the defect determines the shape and properties of the concentrated states such as frequency, polarization, symmetry and field distribution. The investigation of the defect modes in the transmission, reflection and absorption spectra is important to determine optical properties of PhCs.

PhCs are used to make waveguides which widely used to control wave propagation. Regarding the applications of these regular structures, suitable simulation softwares are used to obtain sufficient information about PhCs. Each one uses a special method to compute the optical properties of PhCs, for example, the plane wave method (PWM) is widely used in band structure calculations. The interaction between the radiation field and matter is one of the most fundamental topics of recent research, in which topics about photon absorption and emission, the elastic and non- elastic scattering of the light and the duration of light emitted states are discussed. The principles of the radiation field and its interactions with matter are described using classical electromagnetism and quantum electrodynamics.

In this thesis, the application of PhCs as sensors is analyzed. A novel framework for designing optimized PhC sensors has been also proposed. The complexity of such structures have resulted in the lack of an analytical method to design the structures. Therefore, this framework aims to provide a comprehensive and automatic method to find the best values for the structural parameters without human involvement. The framework is explained with an example of designing a PhC liquid sensor. In the framework, an optimizer called Multi-Objective Gray Wolf Optimizer is utilized. However, a diverse range of multi-objective optimizer algorithms could be utilized. The results show that the proposed framework can design any kind of PhC sensor. Simplicity, being straightforward, and no human involvement are the advantages of the proposed framework. In addition, a significantly wide range of optimal designs will be found which are suitable for general and specific applications.

1-2 Thesis Outline

In the first chapter, PhCs will be briefly introduced, and the band structure and the band gap for the one-dimensional PhCs will be examined. Further, PhCs, their applications and the structure of the two-dimensional PhCs will be specially studied. In chapter 2, a brief review of PhCs will be presented. In chapter 3, a novel multi-objective optimization framework for designing PhC Sensors will be proposed. Chapter 4 is going to utilize the framework for designing new liquid sensor structures. In the last chapter, conclusion and potential future work will be presented.

1-3 History

Ho and his colleagues were the first to introduce a method for constructing a dielectric structure with a band gap [1]. This periodic structure, especially in micron and smaller dimensions, with application in infrared and optical devices cannot be easily constructed. Subsequently, Yablonovich proposed a three-dimensional diamond-shaped cylindrical structure as the first experimental structure, which was able to support an optical crystal band according to theoretical calculations. The first PhC was also constructed by Yablonovich in 1991[2]–[5]. Research continued to find simpler structures in low dimensions, until Lin et al [6] designed a new three-dimensional layer structure with a three-dimensional band gap in a wide range of structural parameters. For the first time, layer structures in the microwave spectrum were made with aluminum cylinders. However, the difficulty to construct three-dimensional PhCs for optical visible waves caused two other research groups to study the band structure of quasi-2D slabs. The results showed that these structures have a band gap within the surface and, due to the general reflection phenomenon, limit the light in other directions. The main success of the structure was its simple construction method. Subsequently, scientists and researchers proposed different construction methods, which will be referred to below.

The "crystal light" term was used by Eli Yablonovich and Saghi Jan in 1987 [2]. However, before that, one-dimensional PhCs were studied in detail as a one-dimensional multilayer periodic matter similar to Bragg's mirrors. Lord Rayleigh began his studies in 1887 by showing these structures with a one-dimensional forbidden band[7]. Today, these bands are used in many cases as high reflectivity layers to increase the efficiency of diodes and mirrors with high reflectivity in laser cavities.

A detailed theoretical study of PhCs by Vladimir Baikov was conducted to investigate the effect of the prohibition band on the spontaneous emission of atoms and molecules[8]. Bikov also thought to use periodic two- and three-dimensional structures[9]. However, the concept of 3D PhC was studied by Oehtaka in 1979[10]. The main motive for Yablonovich was to engineer the density of optical states to control spontaneous emission into PhCs, however, John's [11] was to affect the motion and trap the photons. Increasing the studies on PhCs leads to minimize dimension to micrometers and even nanometers suitable for use in computer and optical communications circuits.

1-4 Photonic crystal (PhC)

In a crystal, atoms and molecules are alternately arranged in three dimensions, and a crystalline lattice is formed by repeating a small base structure of atoms or molecules in space. The repetition of atoms creates a periodic potential for electrons crossing through the lattice. PhCs are formed by repetition of macroscopic dielectric intermediates with a change in refractive index[11]–[14]. A large difference in refractive index with scattering from intermediate boundary creates the same

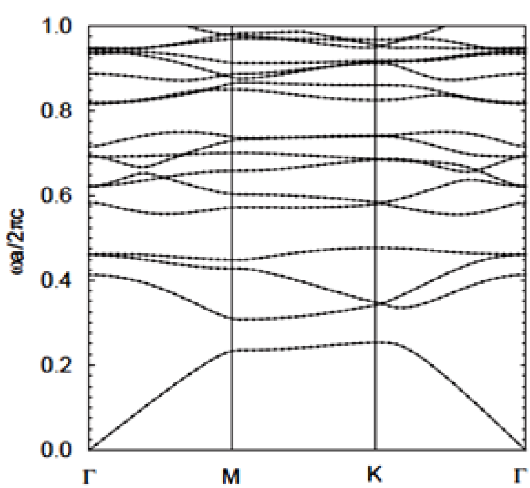

Figure 1- 1: Band structure in a two-dimension photonic crystal lattice [3].

phenomenon for photons, which has an atomic potential for electrons. In other words, periodic refractive index leads to form a band gap in the PhC lattice. The wavelengths of light allowed to propagate are called modes.

The propagated modes concentrate to form a band. Unallowable bands of photonic crystals are called forbidden bands (Figure 1- 1). It is also possible to create energy levels in a forbidden band (defect in photonic crystal), which is equivalent to disrupting the ideal periodicity in a semiconductor crystal lattice with an impurity. Maxwell's equations and the theory of harmonic modes can be used to study electromagnetic wave propagation in a PhC. Development of the PhCs lead to a great deal of development in construction of optical nano- components applied to perfect mirrors, low loss waveguides, resonant microcavities, various filters and optical separators, and so on.

The photonic band gap (PBG) is the fundamental feature of PhC. It does not allow a range of frequencies to pass through[7]. By creating a defect on periodic dielectric structure, leakage mode occurs within PBG which has some features such as small mode volume, strong electromagnetic field confinement, and low extinction loss[8]. However, modifying the structural parameters or filling the air holes of PhC by proper materials are two ways of modifying and engineering the propagation of light on demand. Hence, light flow control is the base of plenty of PhC devices, like filters[9], [10], switches[13], [15], and delay devices[16]. Among all PhC-based devices, sensors are more popular because of their promising characteristics like high measurement sensitivity, ultra-compact size, suitability for monolithic integration, and flexibility in structural design[17]. Furthermore, the PhC-based sensors have various desirable characteristics of optical sensors, like immunity to electromagnetic interference, safety in flammable explosive environment, rapid response speed, and long-distance monitoring. For these reasons, many superior optical sensors based on PhC have been utilized in various sensing applications, such as temperature sensors[18], [19], gas sensors[20], [21], biochemical sensors[22], humidity sensors[23]–[25] and liquid sensors. One structural type of PhC is the PhC cavity (PhCC) which is formed by point defects in the orderly arranged lattices. It exhibits temporal light confinement, strong spatial, and long photon lifetime (particularly, high quality factor Q)[26]. Therefore, there would be more interaction between optical field and material of the defect region. In the case of sensing applications, having more interaction effect causes a boost to an optical mode of PhCC with a resonant wavelength which is unbelievably sensitive to the local variations in its surrounding medium, leading the PhCC to work as a high-sensitive optical sensors[27].

PhCs are generally classified to three categories as one-, two- and three-dimensional crystals. The periodic refractive index in one, two or three dimension forms a one-, two- or three-dimensional PhC, respectively (Figure 1- 2). These crystals are resulted from similarity of the Schrödinger equation in solid state physics and the Helmholtz equation in the field theory in which refractive index plays same role as electric potential. Thus, the performance of PhCs (structures with different refractive index) against photons is similar to that of semiconductor crystals (structures with alternating electric potential) against electrons[12].

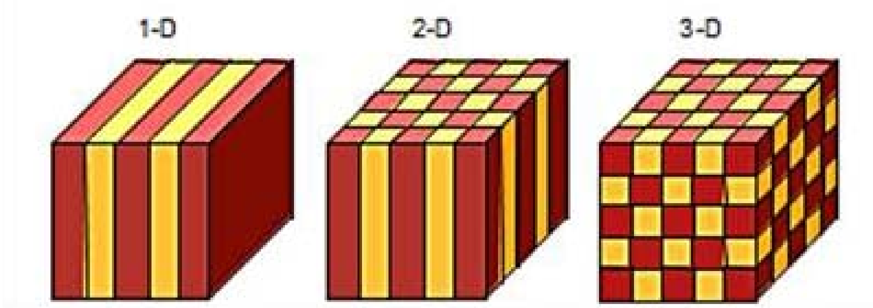

Figure 1- 2: One-, two- and three-dimensional photonic crystals [9].

Since the dominant phenomenon is diffraction, there must be a relationship between the wavelength and the dimensions of PhC, these dimensions are usually one half of the propagation wavelength. This has made the use and construction of PhCs quite complex[28]; this range is between 400 and 700 nm for a crystal in the visible range.

As known, the relationship between speed (c), frequency (υ), and wavelength (λ_0) is given by the following relationship:

$$\lambda_0 = \frac{c}{\nu} \tag{1-1}$$

Given the relation (1-1), the wave vector (k) can be defined as follows:

$$k = \frac{2\pi}{\lambda_0} \tag{1-2}$$

Then the relation between ω and wave vector k will be as follows:

$$\omega = ck \quad (1\text{-}3)$$

The relation (1-3) is called the emission field dispersion relation of vacuum. If the emission field is assumed to be in a homogeneous environment with a refractive index (η), the dispersion relation in the homogeneous environment will be obtained by Replacement of (1-4) and (1-5) relations in (1-1) and (1-3), respectively.

$$v = \frac{c}{\eta} \quad (1\text{-}4)$$

$$\lambda = \frac{\lambda_0}{\eta} \quad (1\text{-}5)$$

The density of states of emission field in V volume and in vacuum is given by:

$$D(\omega) = \frac{\omega^2}{\pi^2 c^3} \quad (1\text{-}6)$$

The density of states of emission field in a homogeneous environment can be obtained by replacing (1-4) relation in (1-6). The optical properties of atoms and molecules are dependent to D (ω), for example, by taking into account the spontaneous emission of a photon from the electron states of an atom or molecule, the spontaneous emission can be said to be proportional with ω D (ω). If D (ω) is corrected, the optical properties of atoms and molecules will change. PhCs are one of the materials to correct D (ω). The following is shown how optical characteristics of PhCs can be changed to modify the optical properties.

1-5 Point and line defects

Three frequency regions are considers for one-, two- and three-dimensional PhCs. The upper and lower frequency boundaries in which the wave with a frequency associated with this region is allowed to pass through the crystal structure, and the intermediate forbidden band region whose wave is not allowed to propagate in PhC with a frequency within this region. The upper and lower bands can be detected wherever their power is located, that is, in up or down ε areas. Since the region with low ε is often air, the upper and bottom regions of the band gap are known as dielectric and air bands, respectively (Figure 1- 3). This is analogous to the electronic semiconductor band structure in which conductance and capacitance bands surrounded the gap.

If a defect includes a single layer with different width of one-dimensional PhC, then the periodicity will be destroyed. We now focus on propagation along the axis and consider a circuit with frequency ω in the optical gap. As said, the modes with frequency ω will not propagate in the lattice, however, the presence of a defect will now change this fact.

Actually, when there is periodicity k (the crystal momentum, technically) is a good number; when periodicity is broken k stops been a true conserved quantity. However, defects may result in alternate modes within the gap. If the frequency of a mode is within the gap, it diminishes exponentially as it enters the crystal. Multi-layer films operate on both sides of the defect, similar to those of a specific frequency mirror. If two of these films are parallel to each other, the diffused light is trapped and axially between the mirrors jump back and forth. Since the distance between the mirrors is in the order of the light wavelength, modes are quantized. In two-dimensional PhCs, modes with frequency within the gap are not allowed. That means that the density of states, the

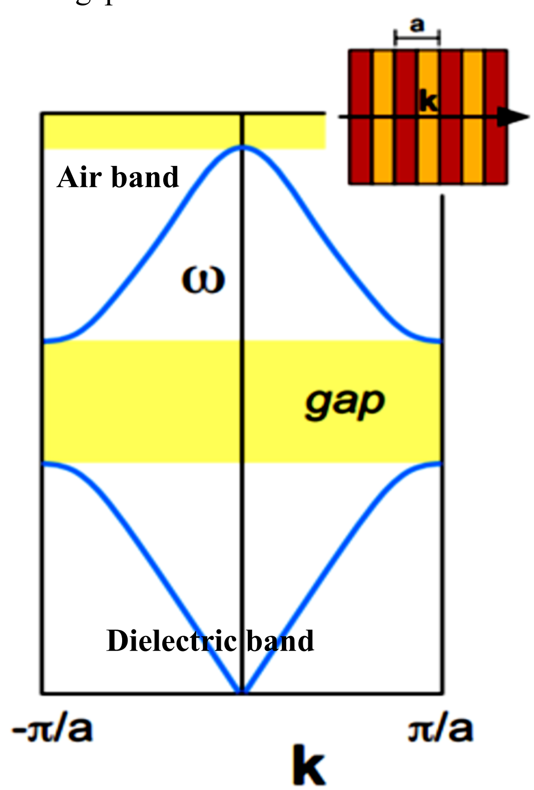

Figure 1- 3: Band structure of a one- dimensional PhC [4]

number of possible modes per unit frequency in the band gap, is zero. Therefore, a disturbance in a single point of the lattice produces a single or close-packed alternate mode in gap.

Elimination of a column may create a two dimensional defect that generates a peak in the density of states of crystal. If the peak is within the gap, then the induced defect state should be transient and the defect mode cannot penetrate in the crystal. Among the one, two, and three-dimensional PhCs, only three-dimensional ones have a complete band gap. A substitution in one-and two-dimension means the light confinement in a planar and a linear defect, respectively. However, it can disrupt the lattice and, as a result, trap the light at a point of the crystal, and as a point defect (Figure 1- 4), caused to add a mode to the gap and create a substituted mode in a three- dimensional PhC.

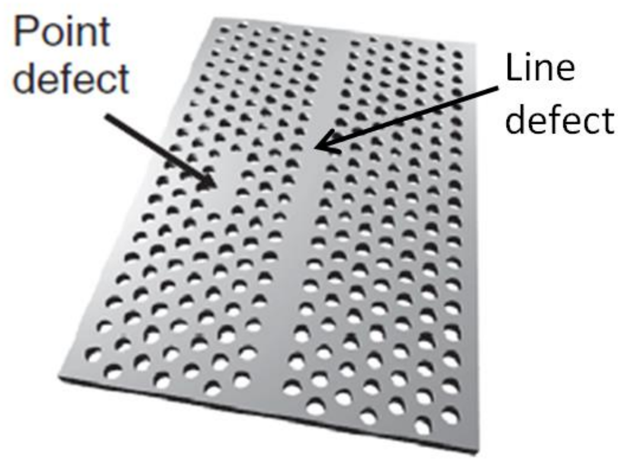

Figure 1- 4: Line and point defect in a planar PhC [27]

There are two simple ways to disrupt a lattice location: addition of an extra dielectric to a place where it does not belong, or removing the dielectric from a point that should have it. The first is a dielectric defect, and the latter is called air defect. Another category of defects is linear defects that are expanded in one direction (Figure 1- 5) and can be considered as linear arrays of point defects.

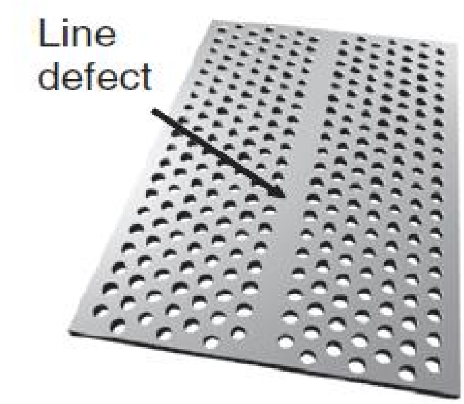

Figure 1- 5: Line defect in a planar PhC [27]

Choosing the appropriate radius and orientation of a linear defect, a defect bar can be created with a frequency within the gap (Figure 1- 6). The states inside of this bar are propagating along the defect but exponentially diminish in the rest of the crystal. By aligning the linear defect with one of the crystal translation vectors, a translational symmetry is maintained along this direction. For this reason, the defect modes can be classified with a defect waveform vector k that determines the phase change along the defect. Such states transfer electromagnetic energy along the defects.

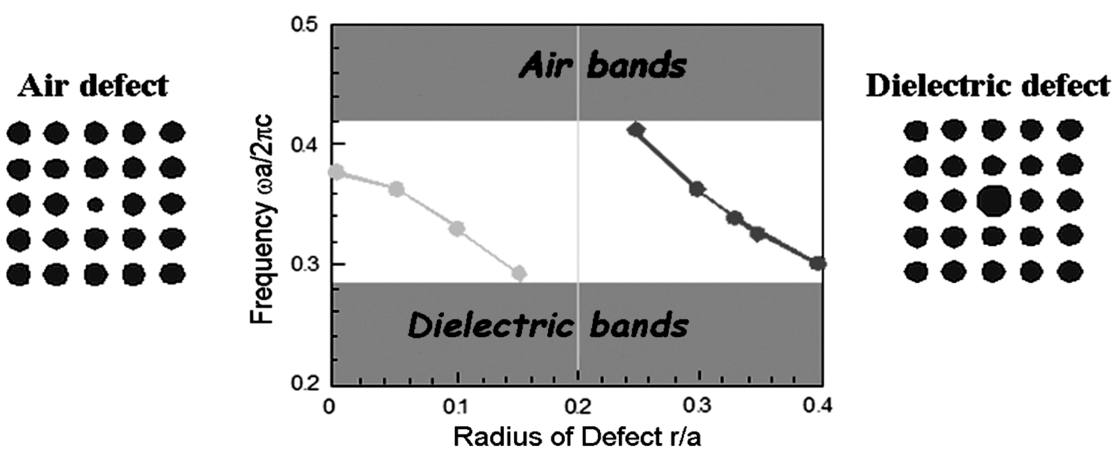

Figure 1- 6: Radius dependence of light frequency [27].

Therefore, it can be said that linear defects are comparable to metal waveguides, in which light is trapped in a pipe with completely reflective walls and dimensions comparable to its wavelength[29].

1-6 Two dimensional PhCs

1-6-1 Two dimensional Bloch states

Two-dimensional PhC is periodic along two coordinate axes and uniform along the third axis. For example of two-dimensional PhCs, a square grid of dielectric rods is shown in (Figure 1- 7).

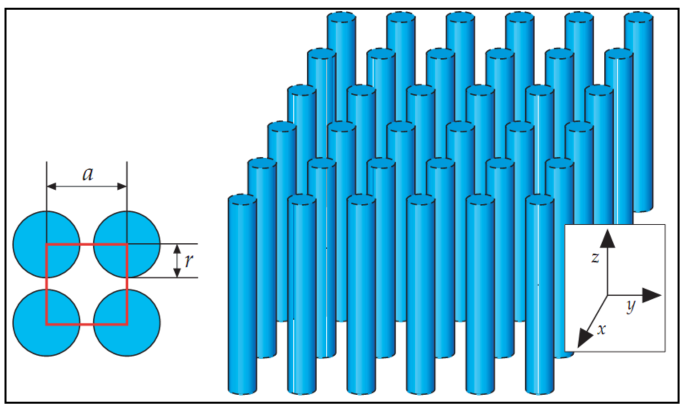

Figure 1- 7: A two-dimensional PhC of square grid of dielectric rods with r radius and ε dielectric constant [8].

The height of the dielectric rods is assumed to be infinite, and since the structure on the x-y plane is periodic, it will has a band structure in this plane. This PhC will prevent propagation of waves inside the x-y plane in certain directions. The symmetry of PhC can be used to determine the electromagnetic modes, because the structure along the z axis is uniform and the electromagnetic modes of the system oscillate on k_z without any limitations in z direction. In addition, since the system in x-y plane has a discrete transient symmetry, it can be focused on the Brillouin zone using the Bloch theorem. The n label has been used to specify the number of the bands. Marking the electromagnetic modes of PhC with k_z, k_p and n will present a new form of Bloch states[10].

$$H_{(n,k_z,k_{II})}(r) = e^{ik_{II}\cdot\rho}\, e^{ik_z z}\, u_{(n,k_z,k_{II})}(\rho) \tag{1-7}$$

In the above relation, the ρ is image of r vector on the x-y plane and u (n, k_z, k_ρ) is a periodic function u (n, k_z, k_ρ) (ρ + R) = u (n, k_z, k_ρ) (ρ) for all the lattice vectors of R. Due to the symmetries in the lattice, electromagnetic modes can be classified into two groups of electric field modes TE (magnetic field perpendicular to x-y plane) and magnetic field modes TM (electric field perpendicular to x-y plane). The band structure for TE and TM modes is completely different, there may be a gap for one polarization, but not for the other within the band structure. In the following, the structure of the two polarization of PhCs, TE and TM, is studied, and the necessary points for reviewing the PhC line structure are discussed.

1-6-2 Square grids of dielectric bars

A two-dimensional band structure of a square grid of dielectric bars (Figure 1- 8) has only a gap for the TE mode.

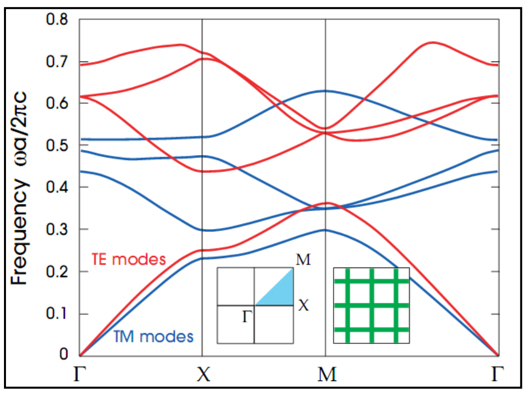

Figure 1- 8: Band structure of square grid of dielectric bars [8]

Patterns of two TE and TM modes will be studied to understand the source of the gap appearance in the band structure between the first and second bands. In (Figure 1- 9), field patterns are shown at the X point in TM mode. It can be seen that for both bands, the field patterns are concentrated in a material with higher dielectric constant. The fields of the dielectric band (first band) are distributed within the horizontal and vertical bars, but only in horizontal regions of dielectric bars are concentrated in the air band (the second band). Therefore, there is no significant jump in band structure in the frequencies, so there is no band gap in TM mode.

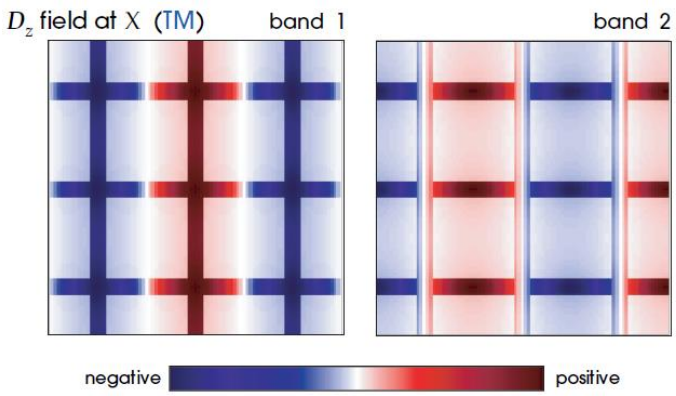

Figure 1- 9: Electric field displacement pattern at x point for TM mode [8]

The density factor for this structure is shown in the (Table 1-1).

Table 1-1: Density factor for structure presented in Fig. 1-9

	TM mode	TE mode
Dielectric band (first band)	89%	83%
Air band (Second band)	77%	14%

On the other hand, for TE mode, the band structure has a gap between the first and second bands. In this case, continuous lines of transverse electric field enter to next area of the dielectric without leaving the material. According to (Figure 1- 10), D (r) field at the lowest band is strongly concentrated on vertical bars of the dielectric material.

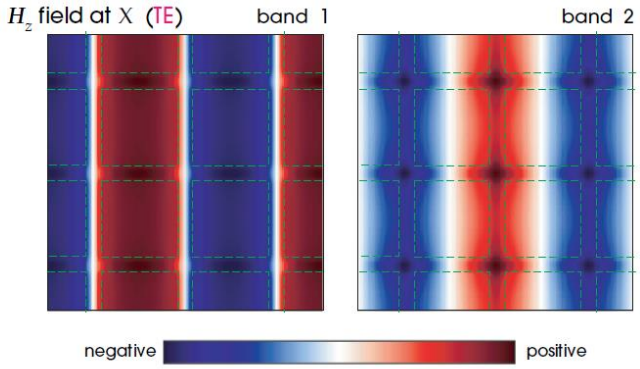

Figure 1- 10: Magnetic field pattern at χ point for TE mode [8]

The D (r) field for the second band to cross from vertical region with high dielectric constant must be perpendicular to the first band. For this reason, some of its energy transmits to the air. In (Figure 1- 10), the maximum displacement of energy is shown in white. Therefore, a large jump of frequencies between the two energy bands occurs. The continuity of the dielectric environment caused to form a gap in TE mode.

1-6-3 Perfect gap for both electromagnetic polarizations

In previous two sections, we used field patterns to study the formation of a gap in the band structure of two-dimensional PhCs for two TE and TM modes. The results make it possible to design a two-dimensional PhC with a gap in both TE and TM modes. Adjusting the size of the PhC combines gap in both TE and TM modes which caused to form a complete gap for all polarizations. According to the above, the band gap in TM and TE modes is created for separate dielectric media and continues dielectrics environments, respectively. At first glance, the design of the PhC with both features seems to be impossible, however, a design with a complete gap for all polarities is possible. A PhC can be designed to connect discrete points using thin dielectric bars (Figure 1-11).

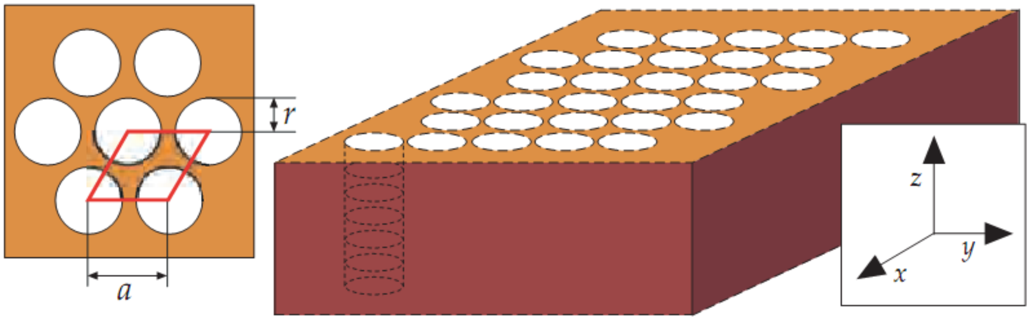

Figure 1- 11: Triangular PhC of air holes in a dielectric environment [8]

(Figure 1- 12) shows a triangular lattice of air holes in a dielectric material. The large enough radius of the holes caused to a similarity of the points between the three holes to the concentrated area with a high dielectric constant. The areas between the holes are also connected using thin dielectric bars.

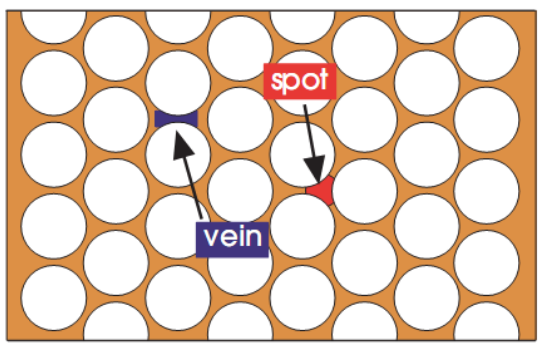

Figure 1- 12: Connection between points and dielectric bars in a triangular lattice [8]

The band structure of this lattice is depicted in (Figure 1- 13), as shown a gap exist for both TE and TM modes. For r/a = 0.48 and a dielectric constant of ε = 13, the gaps of both modes collapse and a complete gap of 18.6% will be obtained.

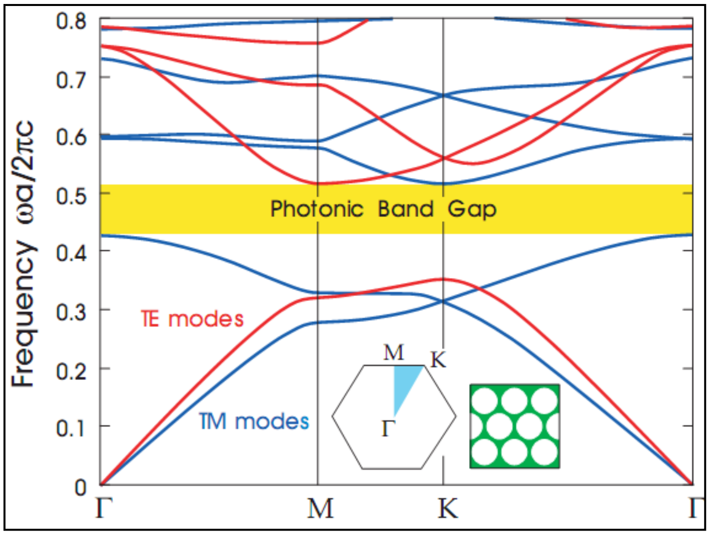

Figure 1- 13: The band structure of triangular lattice of holes in a dielectric environment [8]

1-6-4 Out of the propagation plane

So far, we have specifically focused on the propagated modes in $k_z = 0$ plane. However, for some applications, the propagation method out of the plane is important. (Figure 1- 14) shows the relationship between ω and k_z. For propagation of the waves out of $k_z = 0$ plane the following points should be considered.

1. The uniform structure in the z direction leads to a continuous band without a gap in this direction.

2- When there is no reflection symmetry in the z direction, the modes cannot be purely TE or TM.

3- The bands will be flat with increasing k_z, however in $k_z = 0$, the lowest mode will expand along the wide range of frequencies. With increasing k_z, the lowest mode will be flat and band width will tend to zero.

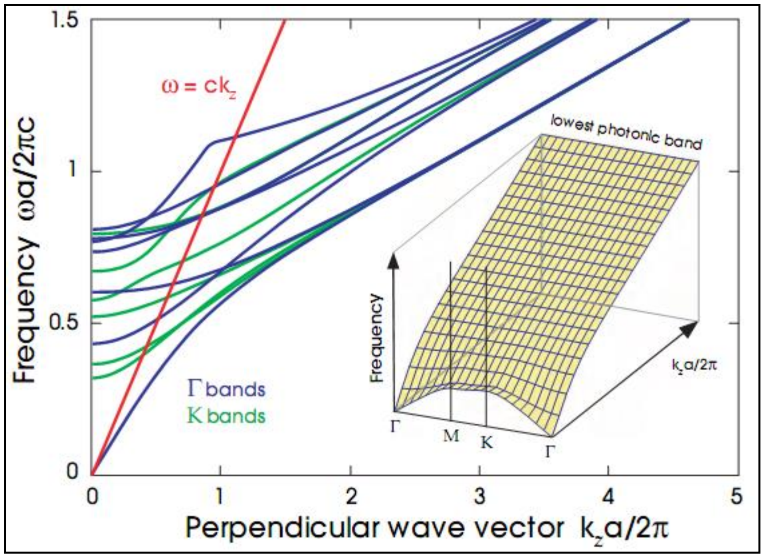

Figure 1- 14: Band structure out of $k_z = 0$ plane for triangular lattice of air holes in dielectric material [8]

Chapter 2 Literature Review

2-1 Application of PhCs

2-1-1 Photonic crystal waveguide (PhCW)

As seen, point defects in PhCs can be used to trap the light. Also, using linear defects, light can be guided from one location to another. The light with frequency in the band gap range is limited to propagate along the waveguide. The ability to prevent light propagation for certain frequencies within the crystalline structures provides new methods to control light and design integrated optical devices. Creating a periodic one-dimensional disorder in a row of PhCs will create a one-dimensional waveguide. When photons with frequencies ranged in optical band gap are released to the defect bands, they cannot propagate into the PhC structure, therefore, they reflect between two regions surrounded the defect and propagate.

A linear disorder (one dimensional) in the PhC structure is created by increasing or decreasing the size or displacement of one or more rows of PhC cavities and resulted in a refractive index difference between the defect region and PhC structure to form a PhC waveguide. Visible light can be driven by optical fiber cables based on the internal reflection, but a sharp curvature of the fiber caused to escape from corners of the fiber for large angle of incident lights. PhCs can be used to limit light even in sharp corners because they do not operate on the basis of internal reflection.

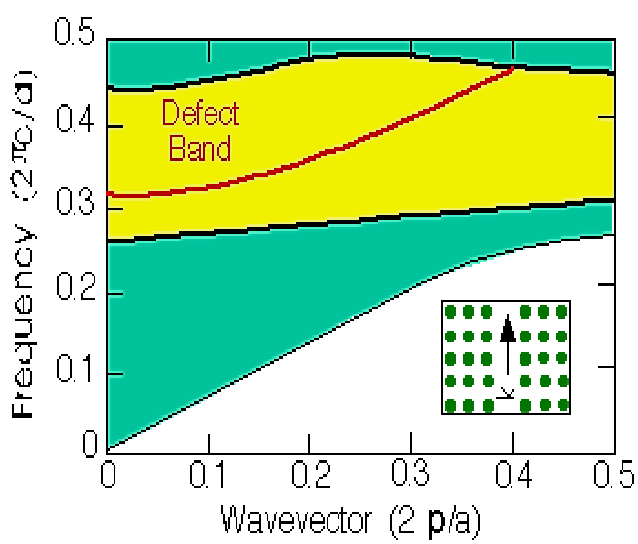

Figure 2- 1: Band structure of TE mode for a waveguide of square lattice and presence of defect mode in PhC structure [27]

For this reason, a PhC waveguide can be used to transmit a monochrome light. In fact, the waveguide is an empty space between the fully reflective walls. (Figure 2- 1) shows TE mode of imaged band structure for a waveguide of square lattice of dielectric bars in air. The green region contains states that can propagate in all crystals, and the red line corresponds to a guided mode that can freely move in the waveguide channel[29].

The main source of light escape can be returning light from the waveguide input. This suggests that PhC can be used to propagate light even from the sharp edges, even 90 ° bending. When the radius of bending curvature is less than the wavelength of light, almost all of the introduced light can exit (Figure 2- 2) [30].

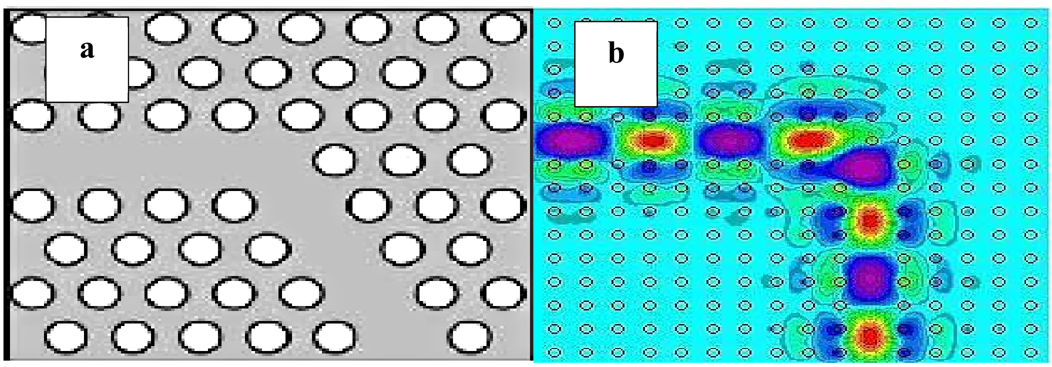

Figure 2- 2: a) a bend in a two dimensional PhC lattice and b) component of field related to a 90° bend in a two dimensional PhC [29]

These structures are generally created by combining Bloch modes of PhC sheets with different propagation constants in a direction that symmetry is broken. These Bloch modes of PhCs are essentially located at high or low frequencies of the gap which are called capacitance and conductance bands, respectively. These modes are transmitted to frequencies within the gap in presence of defects. A small increase in the effective refractive index of PhC structure (creating a defect with a refractive index larger than PhC) will transmit the Bloch modes below the gap to forbidden band called as donor mode in similarly with a decrease in the effective refractive index of the PhCW receiver modes. Since the effective waveguide index in the conduction region (the waveguide core) is lower than the surrounding area (cover), the waveguide modes are restricted by forbidden band of PhC and the effect of PhCW receiver modes on conductivity is negligible. Therefore, only a core with a higher effective refractive index respect to the cover is allowed, and PhCW will restrict in perpendicular plane to PhCW. The waveguide modes of donor PhCWs always occur in materials with high dielectric constant. These modes leads to more optical constraints and lower emission losses, which makes them suitable for the integrated circuits. The receiver modes of PhCW result in higher density of light energy in lower index materials which is attractive for sensitive optical integrated circuits application. A typical example of PhCWs is a case in which a waveguide is created by removing a row of optical cavities and are known as W1-type PhCWs as the simplest and most common types of PhCWs. (Figure 2- 3) shows this type of waveguides.

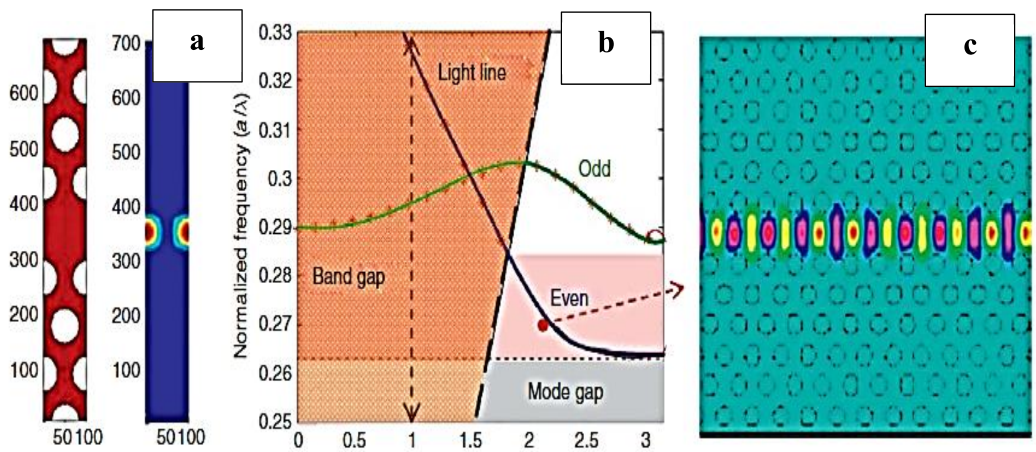

Figure 2- 3: Band structure of TE mode for w1-type PhCW, a) unit cell of PhCW, b) band structure of TE mode for PhCW in energy band of PhC and c) field pattern of conductance mode of PhCW [29]

(Figure 2- 3)(b) Shows a single cell of a w1 type PhCW for TE polarization mode. In a w1-type PhCW, even modes provide larger bandwidth in a single-mode transmission. The bandwidth is limited on one side by the light line and on the other side by the forbidden band mode. A light wave which has the wavelength within the bandwidth of even modes propagates with lower group velocity.

2-1-2 PhC cavities (PhCC)

For the first time in 1989, PhC cavities including two Bragg reflection distributions were presented. However, the concept of a forbidden optical band has been introduced in 1987 even before appearance of a vertical cavity. In fact, a laser cavity acts as a protective box that can hold a photon inside a limited space for a long time. PhCCs can limit photons in a very small space. The quality factor of PhCs can be very large, making them attractive for laser applications, PhCCs can be formed in the range of band gap. The defect mode in the bandgap region results from the presence of a defect in PhC structure. Allowed modes within the forbidden electromagnetic band in PhC sheet are introduced by one or more defects resulting from a disturbance in the periodic structure of crystal. This phenomenon is similar to formation of deep levels in electronic forbidden band of a solid, due to impurities.

2-2 Optical properties and sensing principles of PhCCs

There are several categories of PhCCs which include ring cavity[31], [32], Ln ($n \geq 3$) cavity[33]–[35], mode-gap cavity[36], H_m ($m = 0, 1, 2$) cavity[37], [38], and shoulder-coupled cavity[39], [40], as shown in (Figure 2- 4).

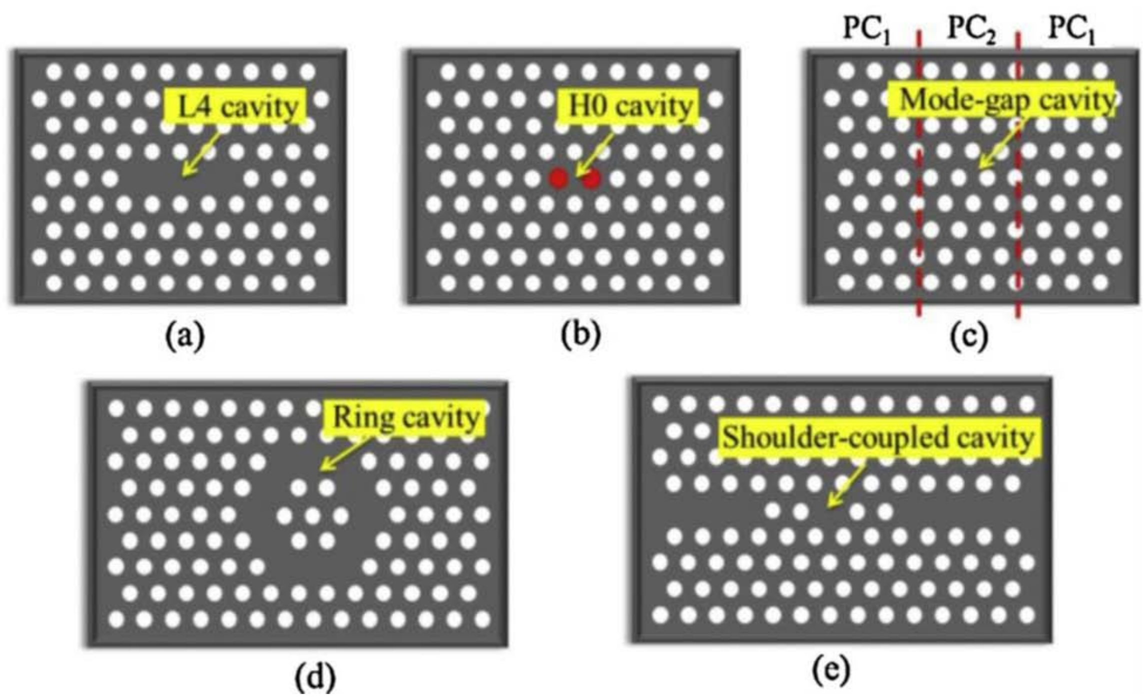

Figure 2- 4: Schematic structures of (a) L4 PhCC, (b) H0 PhCC, (c) mode-gap PhCC, (d) ring PhCC, and (e) shoulder-coupled PhCC [40].

Considering the shoulder-coupled cavity which published in Ref.[40] as an example, sensing principle and the resonant properties of this PhCC will be introduced. First of all, some of PhC waveguide (PhCW) property is introduced which can be generated by removing some air holes from the perfect PhC, as shown in (Figure 2- 5)(a), where r is radius of the air hole, a is the lattice constant, h is the slab thickness, and d is the waveguide width. If the light which exist in PBG is confined in two directions, horizontally and vertically, then it could be guided in the line waveguide. Horizontally confinement of propagated light is due to PBG of PhC and vertically confinement is due to total internal reflection which comes from the RI differences between layers.

(Figure 2- 5) (b) demonstrates the calculated electric field distribution of PhCW when the working frequency of transmission light is located in the PBG, which is simulated by using Rsoft[41].

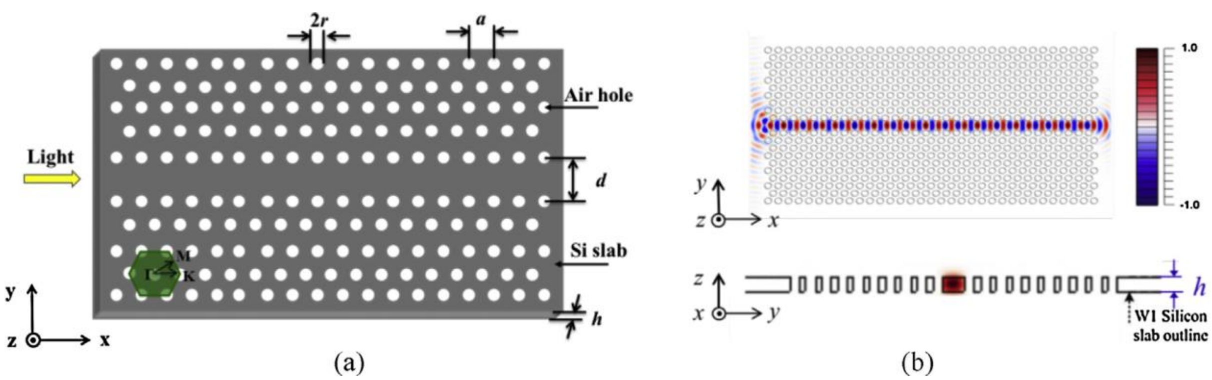

Figure 2- 5: Schematic structure of PhCW (a) and its corresponding electric field distribution (b) [40].

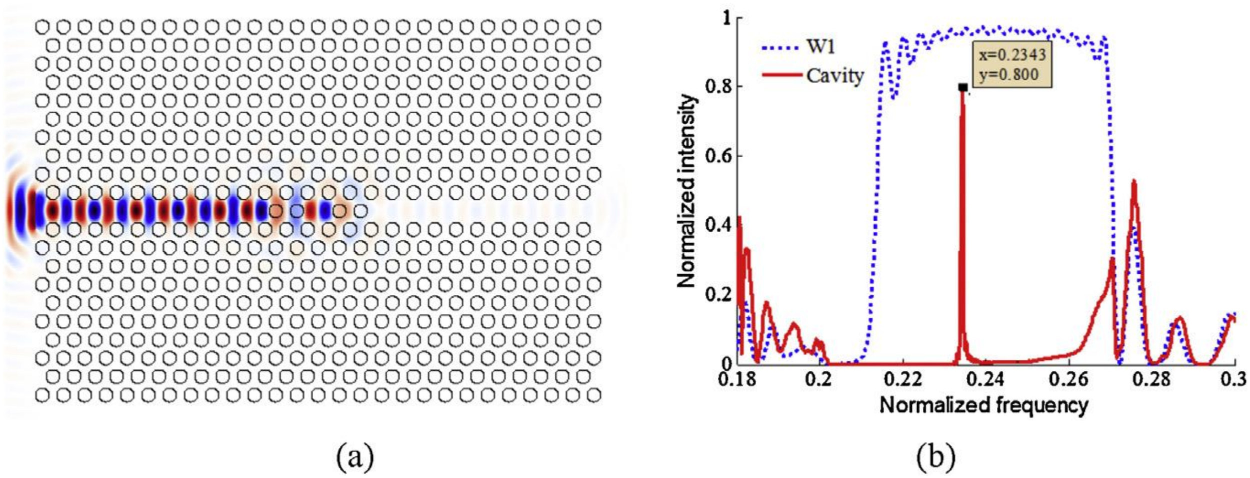

Figure 2- 6: a) Electric field distribution of a shoulder – coupled PhC and b) transmission spectra of w1 type PhCW and shoulder – coupled PhCC [40].

2-2-1 Holey crystalline fibers

Regular optical fibers confine light based on total internal reflection, and thus were inherently weak and only could be used to relatively short wavelengths. Holey crystalline fibers provide single mode performance by conducting the light in a hollow core surrounded with a microstructure coating that is created by a regular period of air holes in silica (Figure 2- 7).

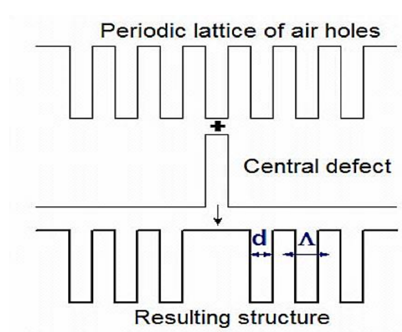

Figure 2- 7: Schematic demonstration of a refractive index [42].

The holey crystalline fibers rely on two-dimensional PhC composed of regular array of air holes. The internal reflection pattern is not allowed in holey crystalline fibers, because in this case the coating index, combination of pure silicon and air, is higher than the air index and the light conduction only depends on the Bragg scattering (Figure 2- 8). When a central defect is created in PhC, the light at certain wavelengths does not allow to pass from the optical forbidden band and therefore it is confined in the defect.

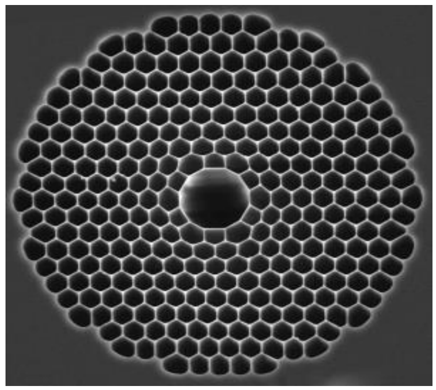

Figure 2- 8: PhC holey fiber [42]

Since propagation of the light in core with lower refractive index is only based on the optical forbidden band characteristic, fibers called as optical forbidden fiber. Optical forbidden fibers, PhC covers act as a mirror and caused to place more than 99% of the light power in the air. Therefore, the light in the wavelength range of forbidden band's confined to the core and propagates along the fiber with low loss (Figure 2- 9). PhC holey fibers have the ability to reduce extreme loss because the light is propagated in the holey core. Losses as small as 1/2 dB / km have been achieved with a core in the order of 7 to 19 unit cells in PhC holey fiber and reducing the coincidence between the basic modes and the glass-air surface modes. The losses as small as 1 dB / km can be achieved in accordance with theoretical predictions [42].

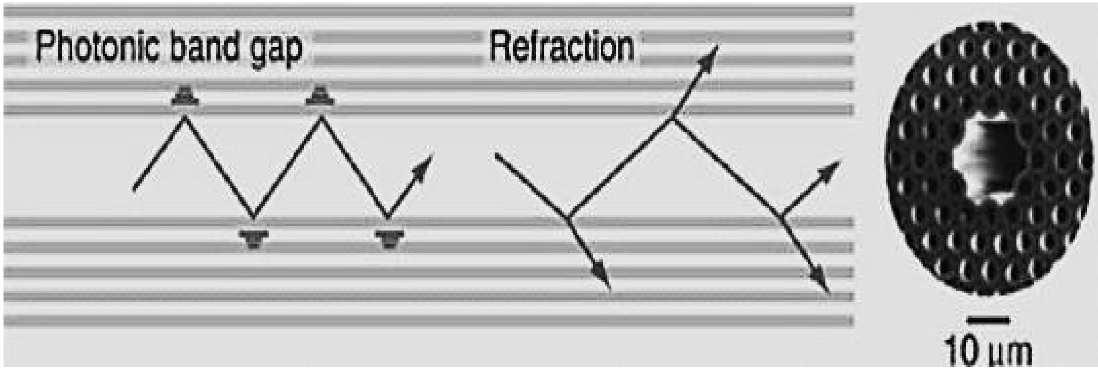

Figure 2- 9: Schematic demonstration of light propagation in PhC holey fiber [42]

2-2-2 Optical sensors based on PhCs

There has been recently a growing interest to design optical sensors for a wide range of sensing applications because of their inherent advantages[43], [44] such as immunity to electromagnetic interference (EMI), small size, lightweight, wide bandwidth, , environmental ruggedness, and low attenuation. Among those, PhC based sensors have been proved to be mainly promising because of their intricate light confinement capability and their compact structure[45]–[49]. PhCs have attracted attention for biological sensing and chemical because of ability to control the material-electromagnetic interaction[50], [51]. They can be used to confine light in the low refractive index (RI) region that provides suitable conditions to strong light-matter interaction to achieve high sensitivity. PhC based micro-cavity sensors generally have a very sharp resonant peak to reduce the detection limits [52], [53] which leads to strong dispersive effects and long photon storage time [52]. This special property makes this structures compact and an attractive platform for RI based sensing applications.

2-2-2-1 PhCW sensors

The main mechanism of performance for PhCW sensors is confinement of electromagnetic field of radiation to the selected rows of holes to achieve maximum interaction of the beam with the small quantity of sample contained in those holes. A liquid or gas flows through the holes of a two dimensional PhCW while propagation of a beam through PhCW is monitored for sample induced changes. As a simple way to manufacture a PhCW, we can remove the air holes within a single row. Low group velocity and very high transmission are important factors to have a propagating mode in PhCW. To insure the effect of material-electromagnetic field interaction, the changes in transmission spectrum of the sample infiltrated the air holes in line defect must be monitored.

2-2-2-2 Gas sensors based on PhCs

Immunity to EMI, rapid response time, room temperature operation and offline monitoring features makes optical sensors a promising device for gas sensing. The integration of microfluidics with PhC technologies leads to having proper gas sensor[55], [56]. The integration of microfluidics with PhC technology promotes optical sensors with very high sensitivity, good limit of detection and detection multiplexing capability. The most widely used technique for optical gas sensing is absorption spectroscopy which is highly sensitive and requires a long absorption length. The light confinement feature of PhCs to enhance the light-matter interaction leads to development of their sensitivity characteristic.

Awad et. al[57] have proposed a PhCW based gas sensor in 2011 for detection of Argon and Helium gases. They reported a 0.6 nm and 0.05 nm shift in cutoff wavelength for Argon and Helium gases, respectively. Specially, interaction between the gas infiltrated in structure and the slow-light mode propagation in it, is resulting in changes of slow-light regime wavelength, and transduced by waveguide effective RI changes. In 2012, Zhao et. al[58] have reported a technique by combining harmonic detection signal processing method for gas sensing and the PhC slow-light waveguide technology. Kumar et. al[59] have proposed a PhC based bi-periodic waveguide structure that an array of super-cavity is used to pass the resonance wavelength through the waveguide. Goyal et. al [60] have proposed a PhCW structure based on ring shaped PhC for gas sensing applications. The enhancement in sensitivity is obtained because of enhancement of guided mode near the core-cladding interface. Benelarbi et. al[61] have reported an improved sensitivity by selective infiltration of adjacent two row of PhCW.

In all the discussed PhCW structures, light is confined in high RI material. However, it can be also obtained in low RI materials[62]–[64]. This is obtained by introducing an air-slot within PhCW structure which has high potential for sensing applications.

Because of inherent trait of PhCC based sensors in detection of low concentration gaseous species, nowadays a tremendous research has also been carried out in their gas sensing ability[65], [66]. Characteristic parameters in gas sensing applications are quality factor, sensitivity, mode volume and signal strength. Mode volume and quality factor are proportional to size of cavity and energy stored inside the cavity structure, respectively. Also sensitivity is proportional to quality factor. The optical mode in the wave guiding medium has to be large enough to get high quality factor.

2-2-2-3 Refractive index sensor based on PhCs

A PhCC has a long photon lifetime as well as shows strong field confinement. That causes an optical mode extend with a resonant wavelength which is highly sensitive to RI perturbations of the medium. For that reason, we could implement many kinds of RI sensors based on PhCC[22], [67]–[71]. Chow et al. were first group to measure the RI change of glycerol-water mixture in 2004. Their method was based on decreasing the radius of one central hole and achieving a quality factor as high as 400. This was happened by monitoring the resonant wavelength shifts in different ratios[22]. It was concluded that for improving detection limit, boosting the quality factor of PhCC and the measurement sensitivity and diminishing the noise level of the measurement should be applied. The structural schematics of PhCCs was summarized in (Table 2- 1).

Another type of waveguides as slot photonic crystal waveguide (SPhCW) was theoretically introduced and experimentally shown[62]. It is formed by opening a slot through the line waveguide of PhCW. It poses unique characteristics of confining and guiding the light in low RI narrow slot with huge field enhancement[72]. Low RI slot and the high RI difference at the interface of Si and electric field discontinuity caused to significant rise in the cavity mode within the slot[73]. In 2008, new PhCC and SPhCW structures were introduced by Yamamoto et. al [74] that local modification of a few of adjacent air holes to the waveguide has formed the cavity.

Table 2- 1: Comparison of different PhCCs that used for RI sensors and their sensing properties [75]

Ref	Schematic structure	Quality factor	Sensitivity (nm/RIU)	Detection limit c(RIU^{-1})	Experiment / Simulation	Published year
[22]	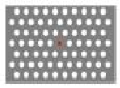	400	200	0.002	Experiment	2004
[67]	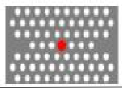	3820	330	0.001	Simulation	2008
[68]	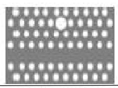	400	155	0.018	Experiment	2008
[68]	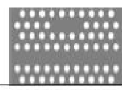	3000	63	0.006	Experiment	2008
[69]	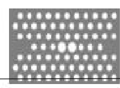	17.890	500	0.0001	Simulation	2013
[70]	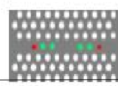	2966	131.7	3.797×10^{-6}	Simulation	2014
[71]	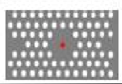	10^7	330	1.24×10^{-5}	Simulation	2014
[76]	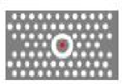	10^7	160	8.75×10^{-5}	Experiment	2015
[77]	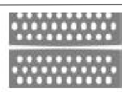	50000	1500	7.8×10^{-6}	Experiment	2009
[78]	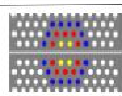	7500	370	2.3×10^{-5}	Experiment	2013
[79]	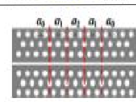	25000	235	1.25×10^{-5}	Experiment	2014

Getting a high Q factor like $2{\times}10^5$ was proved by the simulation results. Di Falco et al.[77], in 2009, illustrated strong RI sensitivity of 1500 nm/RIU and the Q factor as high as 50,000 could acquire in the slot PhCC. Afterwards, some other slot PhCCs[78], [79] were demonstrated their corresponding sensing properties, and their better applications in refractive index sensors are summarized in (Table 2- 1). From the results above, show that PhCCs with high Q and strong optical confinement can be utilized for RI measurement, through the wavelength shift of resonant peak. Guidance for some other sensors such as mechanical sensors, biosensors, gas sensors, and chemical sensors can also be provided by the measurement results as the change of these measurement parameters are able to convert into RI variations.

Table 2- 2: Comparing optical systems which utilized for RI measurement [75].

Optical system	Detection limit (RIU^{-1})	Sensitivity (nm/RIU)	Advantages	Disadvantages	Ref
PCC	7.8×10^{-5}	1500	Flexible in structural design, Compactness, Easy to demodulate, Integration	Difficulty in fabrication, Temperature cross-sensitivity, Large coupling loss	[77]
SPR	5×10^{-6}	2000	Good flexibility and extensibility, High sensitivity	Temperature cross-sensitivity, Difficulty in fabrication	[80]
Modal interference	1.74×10^{-6}	580	Easy to fabricate, Low cost	Interferences of multiple modes (non-linear output)	[81]
Evanescent wave	10^{-6}	700	Good flexibility and extensibility, Simple structure	Influence to light intensity fluctuations, Lack of robustness	[82]
F-P cavity	1.64×10^{-5}	670000	Simple structure, Low cost	Difficult to demodulate, Lacks of flexibility and extensibility, Uneasy to control cavity length	[83]

As for RI sensor, there exist more optical systems, such as modal interference[81], Fabry–Perot (F–P) cavity[83], evanescent wave[82], and surface plasmon resonance (SPR)[80]. (Table 2- 2), compares the pros and cons of these optical systems and summarizes the best values of detection limit for their applications in RI measurement. Romano et. al. in 2017[84] have presented a new RI sensor based on the bound state in the continuingly resonance shift excited in a PhC membrane. Using a microfluidic cell could control the injection of the fluids with different RI over the PhC surface. Observing the shift of high Q factor resonances excited within the PhC open cavity as a function of the RI of the test liquid. The minimal loss-free optical equipment and an excellent stability prepare a new way to fulfill high performance in sensing applications. (Figure 2- 10) shows resonance wavelength shift corresponding to two different indices of 1.4000 and 1.4480.

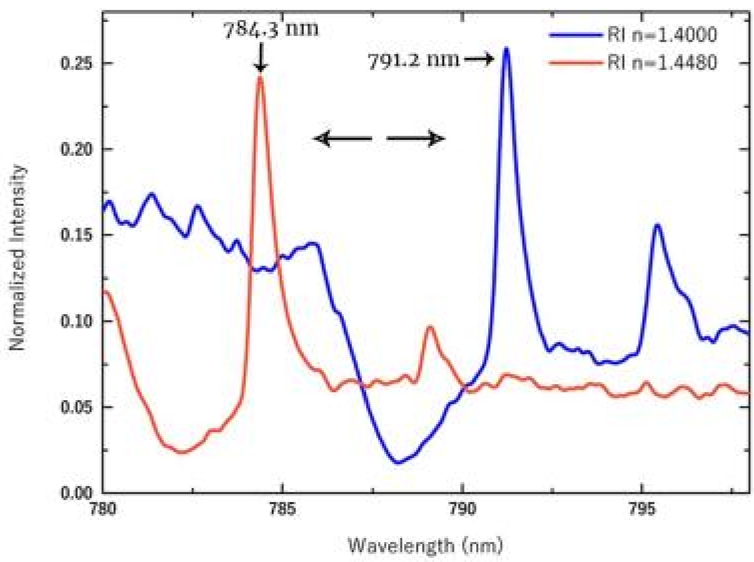

Figure 2- 10: Resonance wavelength shift corresponding to two different indices; n = 1.4000 and n = 1.4480. the resonance is highly sensitive to the refractive index of the fluids over the PhC and this involves a rapid change of the peak position [40].

2-2-2-4 Biochemical sensors based on PhCs

Since the concentration of the biochemical sample is directly related to the RI of the alloy, biochemical sensors are currently measured in terms of RI by analytical interaction with an optical field as a main mechanism. Constraints on a biochemical sensor mainly depends on the targeted area from environmental monitoring to biomedical applications as sensitivity, efficiency, miniaturizability, low latency, manufacturability and cost effectiveness as commonly desired features. Various configurations of the biochemical sensors are recently proposed such as, photonic crystal fiber (as holey fibers) sensors[85], [86] in which the electric field is confined in the core region surrounded by air holes as a location of the measured sample. The interaction between the electric field and material occurs within the air holes. Sensitivity of this type of sensors is generally very low due to rapid decaying of the penetrated electromagnetic field to the sensing region. To increase the sensitivity, longer PhC fibers can be used, however different issues should be considered as increased sample quantities, greater latency and uniform diffusion of the sample within the air holes[87]. By developing of PhCC based on RI sensors, several PhCC based biochemical sensors were introduced[75]. In 2005 Chakravarty et al. used a L4 PhCC coated ion-selective polymer to measure cation and anion concentrations[83]. It was also showed by Lai et al. and Zou et al. as separate works that increasing length of the cavity would almost enhance Q factor of the cavity ten times and improve the shift of resonant wavelength while keeping its compact size characteristics[88], [89]. Then in 2007 Lee et al. reported ability of a PhCC resonator with only one point defect to separately detect very small protein molecules, a gold nanoparticle or anti-biotin in a low active sensing volume[90]-[93]. Finally, in 2010, Hsiao et al.[94] demonstrated for the first time that the ring PhCC is highly sensitive to control the reaction kinetics and low concentration of protein.

2-2-2-5 Surface wave sensor based on PhCs

Nearly all PhC based sensors exploit the photonic stop band or the properties of the Bragg reflection. Nevertheless, some PhC based sensors take benefit of the surface wave on the periodic structure for sensing. Such a sensor was utilized by Villa et. al[95] to characterize thin films. There is a direct relationship between higher sensitivity and advantage of the sensor over surface-plasmon polarization waves on a metallic surface. TE polarization is more useful for sensing applications when TM polarization has the Brewster angle at a certain angle of incidence. The photonic band structure of 1D PhC is shown in (Figure 2- 11). Dispersion curve for the surface waves calculated utilizing supercell method appears only in the 1st and 3rd band gap as shown with dashed lines in the figure.

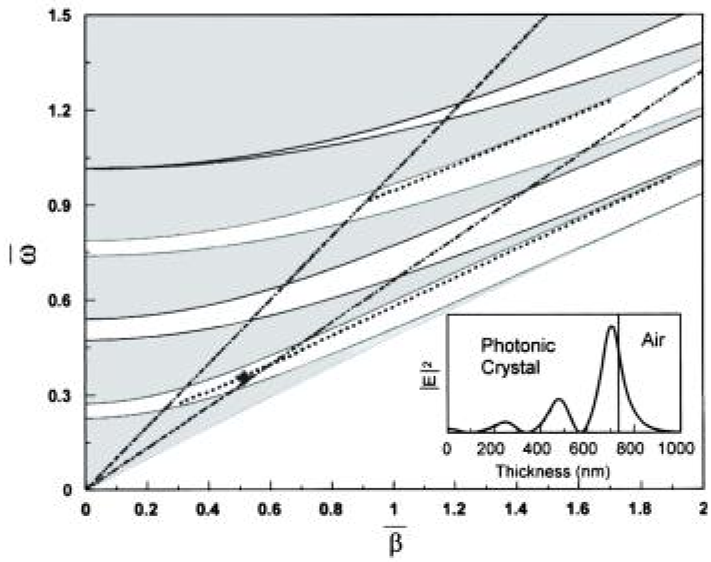

Figure 2- 11: Band Structure of TE polarization. The light lines for glass and vacuum at angle of incidence of 85° are given by lower and upper dashed lines, respectively. The area limited by these lines presents the region where it is possible to excite surface waves by TIR [93]

2-2-2-6 Temperature sensor based on PhCs

Temperature sensors can be based on PhCs. Observation of a shift in the Bragg peak or photonic stop band due to changing the temperature of the material constituting the PhC is the basic concept of the temperature sensor. PhCs were generally fabricated using SiO_2 spheres derived from the sol-gel chemistry. The optical properties of the PhC change when the RI is varied. It can act as a temperature sensor, if the RI changes with the temperature.

2-2-2-7 Oil sensor based on PhCs

Oil sensing uses oil invers opals made of carbon. The color change of the inverse opal is visible even to the naked eye when the oils are infiltrated. The response time for PhC based oil sensors is usually 30s longer than other oil sensors. Regenerating efficiency of the inverse opal for the diesel and the cyclic absorption performance is shown in (Figure 2- 12) that for each cycle, the device was stable for nine cycles similar to other oils and the recovered amount was the same as the absorbed amount.

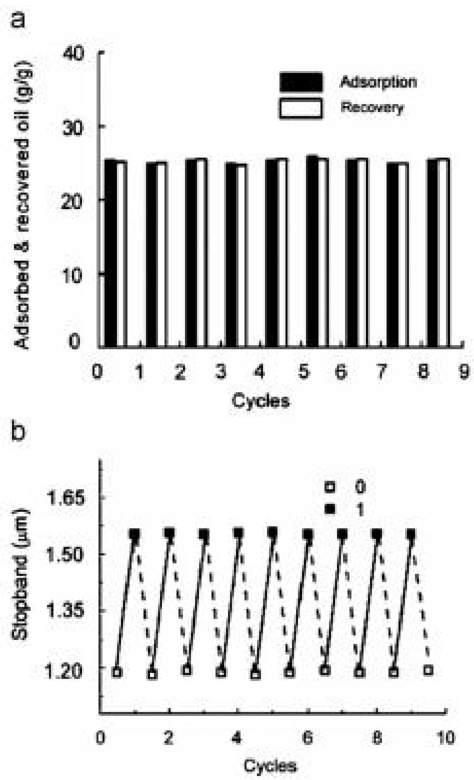

Figure 2- 12: Recycling performance of the PR inverse opal (a) Mass recycling efficiency. (b) Stop band position cycling. 0 and 1 represented the status of the PR inverse opal before and after oil sorption, respectively [93].

2-2-2-8 Humidity sensor based on PhCs

For sensing species in humidity variations in the environment by directly exposing to the ambient atmosphere, PhCs fabricated with a soft hydrogel can be applied. The response time for humidity sensors based on PhC hydrogel is of the order of seconds because they are thin film and can be utilized only in very restrictive environments. Their small size and flexibility are also attractive due to the fact that they use in applications where other sensors are not compatible.

2-3 Construction methods of PhC

Since the smallest discrepancy (even as small as a few nanometers) in the sizes of the fabricated PhC devices can result in a significant effect on the optical properties, it is highly important to reduce this discrepancy between the fabricated PhC device and the original design as much as possible, or in the other words, to maintain the fabrication induced disorder at an acceptable level. Duneau et al.[96] presented a new method to obtain three-dimensional PhCs by chemical vapor deposition (CVD). They also optimized the geometry of the interferometer of the proposed method by Campbell et. al in 2000[45] with respect to polarizations and relative intensities of the beams. They show that a laser source with short pulses could induce a suitable thermal contrast on a convenient substrate in order to grow a three dimensional PhC by CVD.

Up to here, all of the proposed methods have benefits and drawbacks. Self-assembling methods are very cheap and do not need many complicated laboratory equipment. The inability to monitor the number of defects in the crystals as well as the difficulty in getting crystal symmetries other than the face centered cube (fcc) are two cons of the self-assembling routes method.

2-3-1 Holography

Optical holography is an ideal and suitable method for making high-power PhCs in a large area in comparison with the EBL method. Using a natural negative photoresist, a highly concentrated ultraviolet beam is used to create linear defects in light crystals produced by optical holography[97]. In single holographic use, there are following problems:

• Sample is exposed to ultraviolet radiation after the holography and before rising. Therefore it is difficult to separate areas exposed to radiation from unexposed ones.

• Another problem is that exposure to UV radiation does not only create defects, but also changes the size of the cavities near the defect area, which is not the goal.

2-3-2 Anodization method

Aluminum anodization in an acidic environment causes to create cavities between 5 to 200 nm in size, the gap between the cavities can range from 12 to 500 nm. If the annealing condition is appropriate, the created cavities will have a six-fold arrangement. The length of the cavities depends on the duration of the anodization and can reach more than 200 microns. Due to its low absorption, good thermal stability and easy transportation, cavity alumina structures are good materials for the production of two-dimensional PhCs in the visible and infrared regions. The alumina bandgap is about 5-9.5 eV. The array created from the cavities provides the proper conditions for the construction of two-dimensional PhCs. The construction of the regular arrays of cavity alumina includes one step and two step methods. (Figure 2-14) depicts SEM image of a PhC with a Cr defect and InP defect after removing the remained Cr layer.

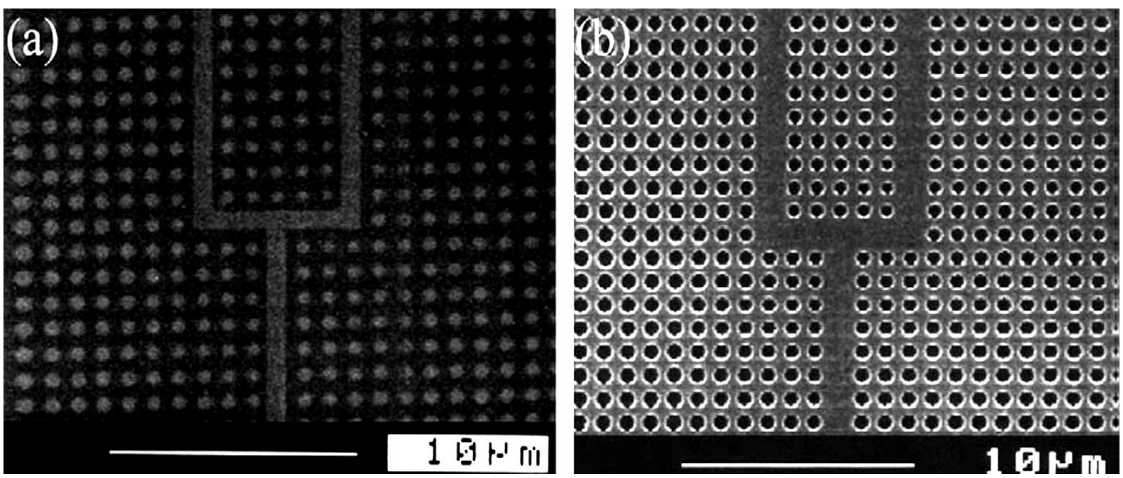

Figure 2- 13: SEM images of a PhC with (a) a Cr defect and (b) InP defect after removing the remained Cr layer [98].

2-3-2-1 One-step anodization method

In this method, using a lithographic method on the silicon nitride substrate, pattern of the holes with a six-order arrangement is initially developed. These holes are used to press the shallow holes on the aluminum surface (Figure 2-15). Then the holes are deepened using the anodizing method, so that the sample as anode is placed in a 1% phosphoric acid solution, and a voltage of 195 v between the cathode and the anode is applied for 16 h. A platinum sheet is used as cathode.

Consequently, aluminum oxide is formed on the surface of sample and pre-designed holes are deepened due to presence of the field and acidity of the solvent (Figure 2-15).

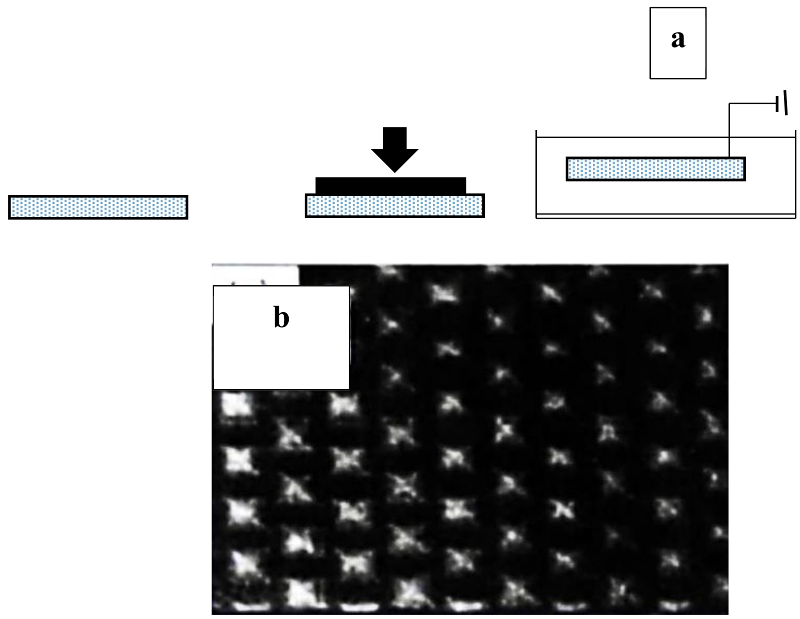

Figure 2- 14: a) The production steps of single alumina PhCs, (b) top view of the aluminum surface after formation of a shallow holes [98].

2-3-2-2 Two-step anodization method

In this method, the anodized alumina is produced by anodizing the aluminum (99.999% purity) in 0.3 M phosphoric acid at voltage of 195 volts for long time. With increasing time of anodization, the order of the holes created on alumina increases and the regular fields are formed. The required time for this anodization is usually between 10 and 30 hours.

After this step, the created alumina is completely removed by combination of phosphoric acid and chromic acid at temperature of 60 ° C. The second step of anodization is repeated with the same anodizing condition of the first step[98].

Since a pattern of the holes created in previous step has been remained on the aluminum surface, new holes are formed in regular areas and a polycrystal is created. The thickness of this polycrystal depends on time of the second step anodization. Radius of the created holes can be increased by chemical phosphoric acid at a temperature of 30 ° C. Therefore, holes with 200-400 nm in diameter can be obtained. If an electrochemical deposition is used, the created holes can be filled with metals or other dielectric materials to obtain wide variety of PhCs. (Figure 2-16) shows cross sectional and top view SEM images of PhC fabricated from two step anodization method.

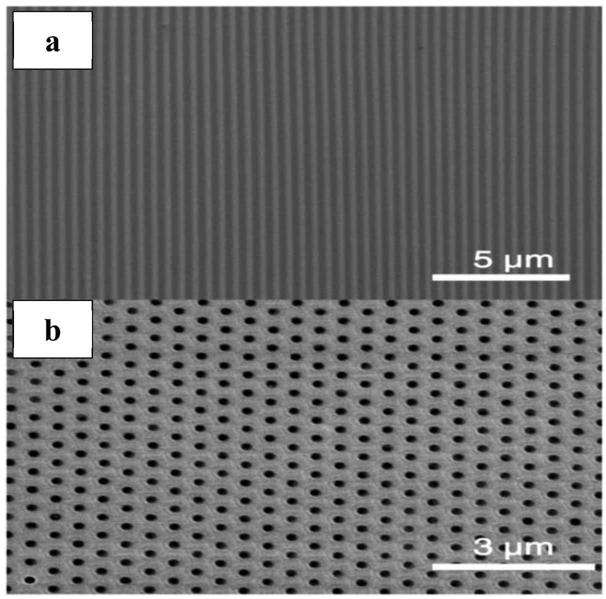

Figure 2- 15: a) cross sectional and b) top view SEM images of PhC fabricated from two step anodization method [99].

2-3-3 Using the HSQ Resist

Typically, the use of polymer resists in PhC production processes has high cost and complexity, and finally, when images are transferred to the bottom of the substrate, poor quality images are created. For this reason, another method is used as resist in this method[98]. Chemical formule of a HSQ is shown in (Figure 2-17).

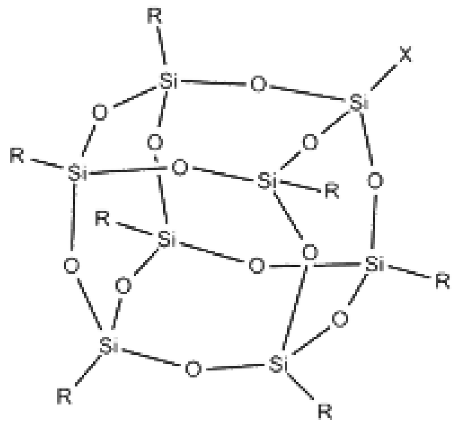

Figure 2- 16: Chemical structure of $(HSiO_{3/2})_n$ [99]

Hydrogen Silisquioxane (HSQ) is an inorganic polymer with the chemical formula $(HSiO_{3/2})_n$. When the pattern is imprinted on it by an electron beam, it can be used to produce a 50 nm object with some features such as a very low roughness and very high power. It is reported that heat or exposure to an electron beam or oxygen plasma caused to break the H-Si bonds and the cage like structure is transferred to the constitutive structure where stronger Si-O-Si bonds are formed, and a more rigid and similar structure would form. (Figure 2-18) shows top view SEM image of the PhC structure on Si created using the HSQ.

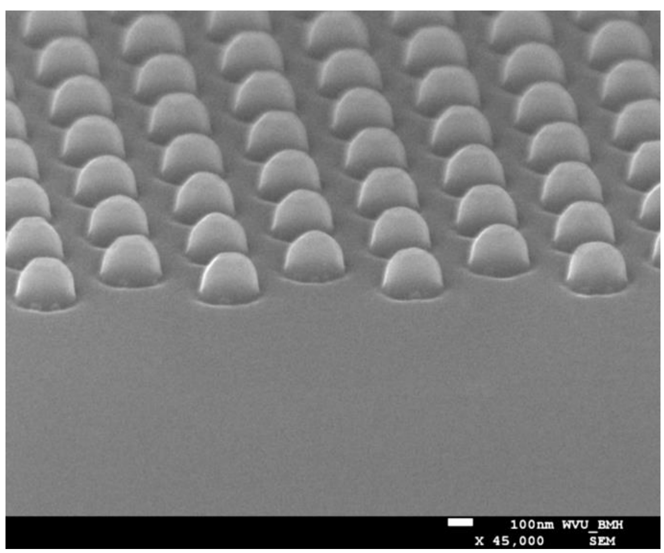

Figure 2- 17: SEM image of final structure produced on Si [99]

2-3-4 Etching

Etching is a nanofabrication process in which a material is removed from any layer of material on the substrate. There are generally two types of etching methods including dry and wet etching. The basic difference between two etching methods is utilizing a liquid chemicals or etchants to remove the materials. There are two major etching mechanisms as physical and chemical etching. In physical etching, the momentum transfer is used to remove the layer. However, in chemical etching, species generated in plasma react with the target to form the vaporizable products. This etching mechanism is similar to wet etching.

As said, wet etching is an etching process which utilized liquid chemicals or etchants to remove the layer from substrate to transfer patterns of photoresist mask into the substrate.

Chapter 3 A Novel Multi-Objective Optimization Framework for Designing Photonic Crystal Sensors[1]

3-1 Introduction

To date, Photonic Crystal (PhC) devices have become popular because they cover a wide range of applications. PhC structures show bandgaps in their spectral transmission performance. By creating defects in the PhC lattice, some leaky modes will be generated in the bandgap region. In other words, these leaky modes provide the opportunity to manipulate the transmitted light [99].

The use of a leaky mode to implement optical filters is one of the most standard applications of PhC structures. This leaky mode provides a very narrow bandpass filter that could be used in a wide range of applications. In this paper, a PhC sensor, based on the optical filtering operation of a PhC structure, is designed with proposed optimization. In such structures, a PhC slab with some air holes is usually considered as the sensing device. Hence, sensing operation is performed by filling the air holes with the designated material and measuring the wavelength shift in the output spectrum of the filter [75].

The main problem inherent with the use of such devices is how to model the internal propagation of light. In other words, finding an analytical equation describing the relationship between the structural parameters and the device output performance is usually very challenging, and in many cases it is impossible. The complexity of the relationship between the structural parameters and the device output performance prevents researchers from proposing analytic methods to design such devices.

The typical method utilized in this field to design such devices is trial and error; that is, the structural parameters are manipulated, then the behavior of the device is observed, and these observations are used to estimate the approximate relation between the structural parameters and the device output. This method requires a huge amount of human involvement with tedious non-systematic efforts. Moreover, the finally designed device is usually far from the optimal one. The trial and error process have been followed in many works in the field of PhC devices [100]-[105].

[1] This chapter has been published in "**M. J. Safdari**, S. M. Mirjalili, P. Bianucci, and X. Zhang, "Multi-objective optimization framework for designing photonic crystal sensors," Appl. Opt., vol. 57, no. 8, pp. 1950–1957, 2018."

Many PhC filter structures, such as PhC cavity [106], PhC ring resonator [107]–[109], and defect-mode based PhC filter [110], have been designed by this approach. More specifically, PhC liquid sensors have been designed manually, leading to far from optimal designs [111], [112].

To solve the problem of the lack of an automatic and comprehensive method for designing PhC devices, the use of artificial intelligence techniques has been proposed. Up to date, the Quality factor (Q) of PhC cavity has been maximized by genetic algorithms [113]–[115]. In ref.[116], a PhC notch-filter has been designed by the particle swarm optimization algorithm. The bend loss of PhC waveguides have been minimized by use of a genetic algorithm[117]. The Extraction ratio and Purcell factor of PhC LEDs have been maximized using a multi-objective grey wolf optimizer [118]. Furthermore, the slow light properties of PhC waveguides have been optimized using similar optimization algorithms [119]–[125].

Recently, comprehensive frameworks for designing PhC filters have been proposed [126], [127]. In these frameworks, the optimal designs have sharp, well-tuned, and low crosstalk output completely, suitable for all filter applications. However, for the application of PhC sensors based on PhC filters, the sensitivity of the sensors must be evaluated and considered in addition to other merit factors. Therefore, in this chapter we upgrade the multi-objective optimization framework for the application of PhC sensor design, in which the sensitivity will be maximized as well as other merit factors. In the rest of the thesis, the process of this framework is explained with the example of designing a PhC liquid sensor.

3-2 PhC Sensor Structure and Related Issues

The proposed structure of the liquid sensor is shown in (Figure 3-1). The structure consists of a silicon slab with some holes in it to form a waveguide and a cavity section. The cavity is made by eight holes. The light will enter the device from the left side. The device has optical filtering characteristics and the spectral transmission characteristic can be examined at the right side output. Filling the holes with Oil (n=1.45) or water (n=1.33) will result in a shift in the output spectral transmission performance. This is the principle for utilizing this structure as a liquid sensor [111], [112].

Before designing the cavity section, it is necessary to design the photonic crystal lattice to have the largest photonic bandgap as a large photonic bandgap provides a wider working wavelength window to design filters. In order to calculate the photonic bandgap of the PhC lattice, the 2D Plane Wave Expansion (PWE) with a slab equivalent index method is utilized [128]. We consider a Silicon-On-Insulator (SOI) slab with 400 nm of silicon, which corresponds to a slab equivalent index of 3.18 for a TE polarized mode [129]. In addition, we consider that the holes are normally filled with Oil (n=1.45) [111]. By sweeping the filling factor (f=r/a, where a is the lattice constant and r is the hole radius) from 0 to 0.5, we conclude that at f = 0.41, the largest photonic bandgap will be achieved. However, we consider f= 0.375 which provides a large enough bandgap and a more mechanically rigid PhC slab. In addition, the central normalized frequency of the photonic bandgap is set to 0.280. Therefore, the lattice constant is $a = 0.280 \cdot 1550 = 433\ nm$.

The idea of realizing a filter by modifying a PhC lattice comes from the fact that introducing defects in PhC lattice causes leaky modes in the photonic bandgap. These leaky modes provide an opportunity to utilize the structure as a narrow bandpass filter. In other words, the leaky mode guides a narrow band of spectrum. Therefore, such structures can be utilized as narrow bandpass filters. To tune the leaky mode, it is necessary to modify the defect structure. In our case, we use holes as a defect region to create the leaky modes.

The more holes involved in defect region, the more flexible the PhC sensor structure is, and the more complex and difficult designing such structures becomes. Here, we consider eight holes as the defect region to manipulate the guided light, which is large enough to provide sufficient flexibility in the design and to show our approach.

In order to evaluate the performance of the device, the output spectral transmission performance is calculated by a 2D FDTD simulation for TE-polarization. As a sample case study, the output of the device is shown in (Figure 3-2). To design a PhC sensor, four merit factors must be considered:

- Ampc: Maximum amplitude of the output in the main band.
- Amps: Maximum amplitude of the output in the sidebands.
- Deviation: The deviation of the central wavelength of the output peak (λ_c) to the defined central wavelength of the channel (λ_O) ($Deviation = |\lambda_{c1} - \lambda_O|$).

- Sensitivity: the ratio of change in the central wavelength of the output peak (λ_c) divided by change in the refractive index of the filed holes ($Sensitivity = \left|\frac{\lambda_{c2}-\lambda_{c1}}{n_2-n_1}\right|$).

The first three factors are three of which are directly related to the performance of the filtering operation [126], [127], while the sensitivity is a criterion specific to a sensor. The above five parameters of Amp_c, Amp_s, λ_O, λ_{c1}, and λ_{c2} are illustrated in (Figure 3-2).

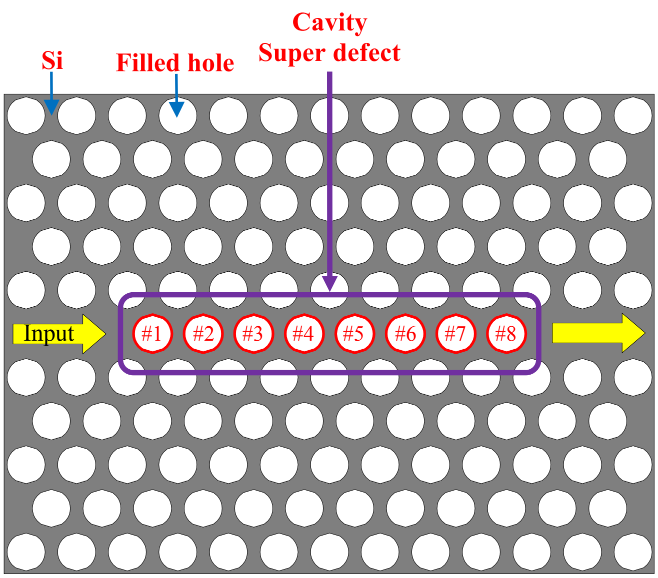

Figure 3- 1: Proposed PhC liquid sensor. Eight holes are used to form the super defect region.

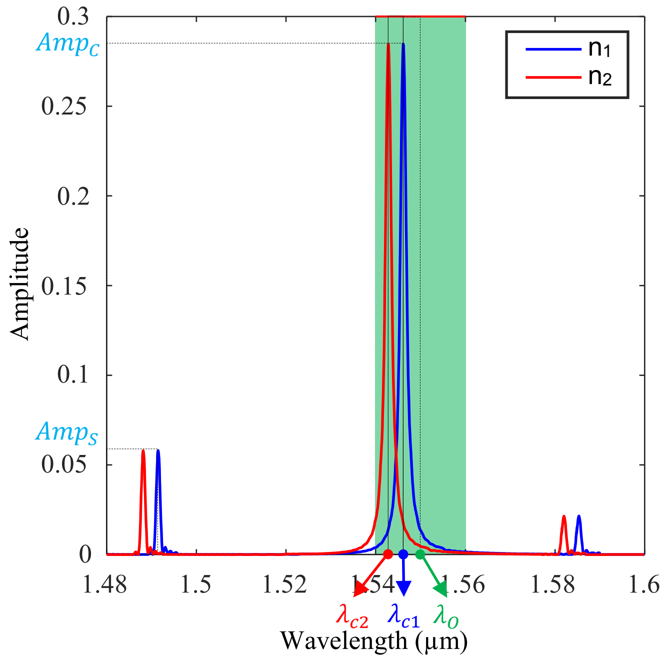

Figure 3- 2: Output spectral transmission performance of an example of a PhC liquid sensor.

3-3 Multi-objective optimization frameworks for designing PhC Sensors

As mentioned before, it is very difficult to find analytical methods; we can sweep the search space or utilize an optimizer algorithm to find the best possible designs. If a design shows high Ampc and Sensitivity with low Amps and Deviation, it means that it is a well-designed PhC sensor. Therefore, the multi-objective optimizer looks for the designs in which Ampc and Sensitivity are maximized while Amps and Deviation are minimized. The framework can be divided in three main modules: Parameters Module, Constraints Module and Optimizer Module, illustrated by (Figure 3-3).

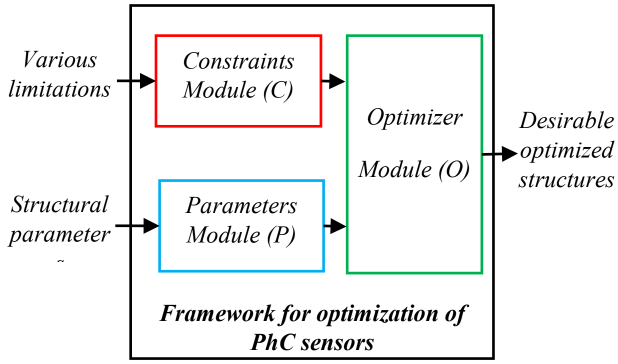

Figure 3- 3: Proposed multi-objective optimization framework for designing PhC sensors.

3-3-1 A. Parameters Module (P)

In this module, the structural parameters must be defined and handled. Therefore, the best values for the structural parameters will be found. The P module for the proposed PhC sensor (Figure 3-1) is given by:

$$P: \vec{x} = \left[\frac{R_1}{a}, \frac{R_2}{a}, \frac{R_3}{a}, \frac{R_4}{a}, \frac{R_5}{a}, \frac{R_6}{a}, \frac{R_7}{a}, \frac{R_8}{a}\right] \quad (1)$$

3-3-2 B. Constraints Module (C)

All of the issues that must be considered during the PhC sensor design are considered in this module. For this case study, two groups of constraints are considered to address the issues. The first group (C1) is related to the parameters ranges. In addition, any manufacturing limitations could be added to this group. The second group (C2) is for checking the validity of the filtering operation of the device. The C module for the proposed PhC sensor (Figure 3-1) is given by:

$$C = [C_1, C_2],$$

$$C_1: 0 \le \frac{R_1}{a}, \dots, \frac{R_8}{a} \le 0.5, \quad (2)$$

$$C_2: Amp_{c1} > Amp_{s1},$$

$$Amp_{c2} > Amp_{s2}$$

The index of 1 and 2 of the C2 section indicates the number of the device simulation.

3-3-3 C. Optimizer Module (O)

Objective functions and an optimizer should be identified for this module: in order to solve the problem with single objective optimization approach, a new merit factor, a combination of the previous merit factors, is defined as:

$$Objective = Amp_{C1} + Sensitivity + \frac{1}{Amp_S + Deviation}$$

The single objective optimizer will try to maximize this parameter. As the Objective is maximized, a higher performance PhC sensor design is achieved. Solving the problem as a single objective problem results in losing many decent designs since the actual answer to multi-objective problem is a set of optimal solutions.

The objectives for the multi-objective optimization approach are Ampc, Amps, Deviation, and Sensitivity. The optimizer should find the PhC sensor structures in which Ampc and Sensitivity are maximized while Amps and Deviation are minimized. Several single- and multi-objective optimization algorithms can be used for the optimizer [130]–[132]. We choose the Single- and Multi-Objective Grey Wolf Optimizer (SOGWO and MOGWO) algorithm for the optimizer [133]–[135]. This algorithm mimics the social behavior and leadership of grey wolves in nature. This algorithm proved its performance in several fields of engineering. The main motivation to choose Grey Wolf Optimizer is the high local optima avoidance, since the problem that is investigated in this work has a large number of variables, resulting in a very difficult task to explore the search space with many local solutions [136].

It is worth mentioning here that there is no single solution for multi-objective problems due to the nature of such problems. A set of optimal solutions (Pareto-optimal set) is the answer to multi-objective problems. They represent the best trade-offs between the objectives [137].

A flow chart of how to calculate the merit factors is shown in (Figure 3-4). The reason why -Amps1 and -deviation1 are considered is that the multi-objective optimizer tries to maximize the outputs of the objective function. By considering the negative value of an output, the direction of the behavior is changed. For Amps1 and deviation1, minimization is required; alternatively, for the negative -Amps1 and -deviation1, maximization is required. Overall, all of the outputs behave in the same direction.

A candidate design, which does not satisfy the conditions that mean a valid filter device cannot be made, is what we call infeasible design. Hence, for such a design the outputs of the objective function must be a set of values, which are much worse than that of the normal valid designs. In this case, we consider Output=-100 for the single objective optimization approach and Output=[-100 -100 -100 -100] for the multi-objective optimization approach. In order to calculate the merit factors, two simulations are required (one with oil as the external medium and one with another liquid). For infeasible designs, we bypass the second simulation, since it does not provide any valuable information.

To simulate PhC structures, the FullWAVE simulation tool of Rsoft which employs the finite-difference-time-domain (FDTD) method to perform a full-vector simulation of photonic structures is used. For the optimizer section, we have developed some Matlab programs to connect Matlab to Rsoft and perform the optimization.

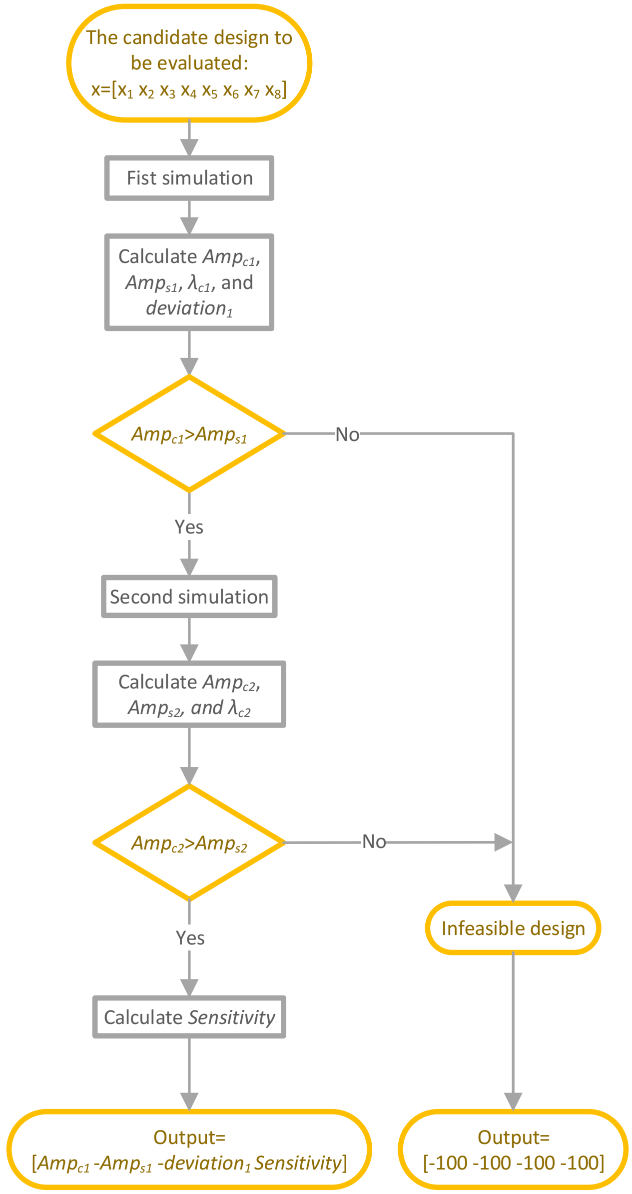

Figure 3- 4: Flowchart for the calculation of merit factors (the objective function of multi-objective optimization approach).

3-4 Results and discussion

After setting up each module, the framework is ready to optimize the proposed PhC sensor. Basically, the optimizer checks different possible combination of the structural parameter values to achieve high-performance design(s).

3-4-1 Single-objective optimization approach:

In order to perform the single-optimization, we have utilized SOGWO with 60 artificial grey wolves and maximum iteration of 400 to approximate the global optimum. The optimizer just considers the Objective function as $Objective = Amp_{C1} + Sensitivity + \frac{1}{Amp_S + Deviation}$ and manipulates the structural parameters until the best value of the Objective is found. The results of single-objective optimization approach are shown as a convergence curves in (Figure 3-5). SOGWO, Particle Swarm Optimization (PSO) [138], [139], and Genetic Algorithm (GA) [140] were utilized to optimize this problem. The comparative study shows that SOGWO gives better results than the others. Therefore, the results of SOGWO with iterations are shown in (Table 3-1), and correspondingly the output spectral transmission performance of the obtained designed filter is given in (Figure 3-6). It is seen that the transmission spectrum performance is better and better with the increase of iterations. It is also shown that single-objective optimization is not the best way to solve this problem. This motivates us to solve the problem with multi-objective optimization approach.

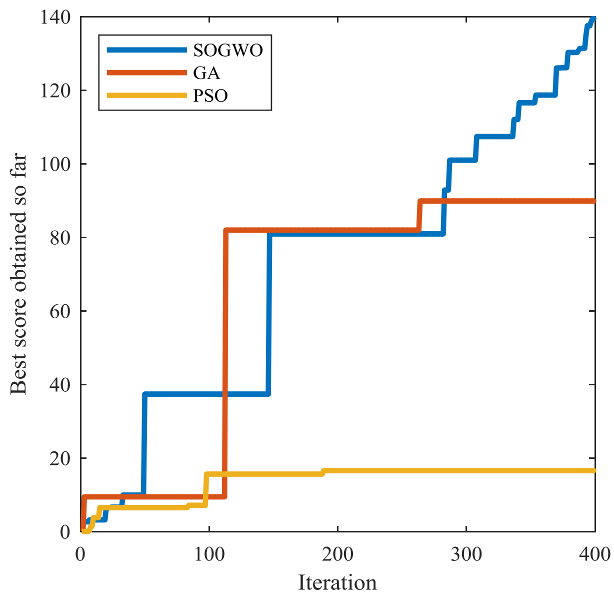

Figure 3- 5: Convergence curve of single-objective optimization approach.

Table 3- 1: Properties of obtained structures with single-objective optimization by SOGWO

Iter	R_1	R_2	R_3	R_4	R_5	R_6	R_7	R_8	Amp_c	$-Amp_s$	-D(nm)	Sen	Obj
1	63	105	154	178	199	32	150	99	0.0003	-0.0001	-0.53	0.285	1.6
3	217	156	175	186	118	3	134	77	0	0	-0.38	0.613	2.1
7	120	164	103	53	0	110	0	27	0.0134	-0.0113	-0.3	0.172	3
20	170	137	26	217	94	131	25	5	0.0788	-0.0052	-0.15	0.277	6.1
22	217	154	0	188	201	68	31	0	0.0721	-0.0018	-0.15	0.24	6.3
24	202	128	27	217	106	217	58	6	0.001	0	-0.15	0.255	6.4
33	162	89	84	217	90	77	40	41	0.0537	-0.0249	-0.08	0.27	9.7
50	217	10	8	180	50	143	46	33	0.0325	-0.0267	0	0.247	37.1
147	217	127	13	150	25	187	51	30	0.0288	-0.0124	0	0.21	80.7
283	214	128	10	134	34	196	62	22	0.0389	-0.0108	0	0.217	92.6
287	217	136	9	139	38	183	71	23	0.035	-0.0099	0	0.217	100.8
308	217	129	8	126	34	203	73	30	0.0495	-0.0093	0	0.217	107.2
337	213	129	8	120	36	208	73	27	0.055	-0.0089	0	0.217	111.8
341	217	140	9	130	35	193	74	22	0.0435	-0.0086	0	0.21	116.4
354	217	139	9	128	35	197	74	22	0.0461	-0.0084	0	0.217	118.5
370	210	148	9	120	36	200	74	22	0.0486	-0.0079	0	0.202	125.8
374	211	148	9	120	37	198	75	22	0.0487	-0.0079	0	0.21	125.9
379	213	141	10	118	35	205	75	22	0.0528	-0.0077	0	0.202	130.1
387	212	144	9	118	35	204	75	22	0.0522	-0.0076	0	0.202	130.5
388	207	143	9	117	36	205	75	21	0.0534	-0.0076	0	0.202	131.1
390	209	143	9	117	36	204	75	22	0.0535	-0.0076	0	0.21	131.2
393	210	144	9	116	36	204	76	22	0.0542	-0.0074	0	0.202	134.9
394	215	146	9	116	36	203	77	22	0.0538	-0.0073	0	0.202	137.3
397	214	145	9	118	36	202	78	22	0.0545	-0.0072	0	0.202	138.5
398	212	145	9	117	36	203	78	22	0.0553	-0.0072	0	0.202	139.3

The unit of Rx is nm.

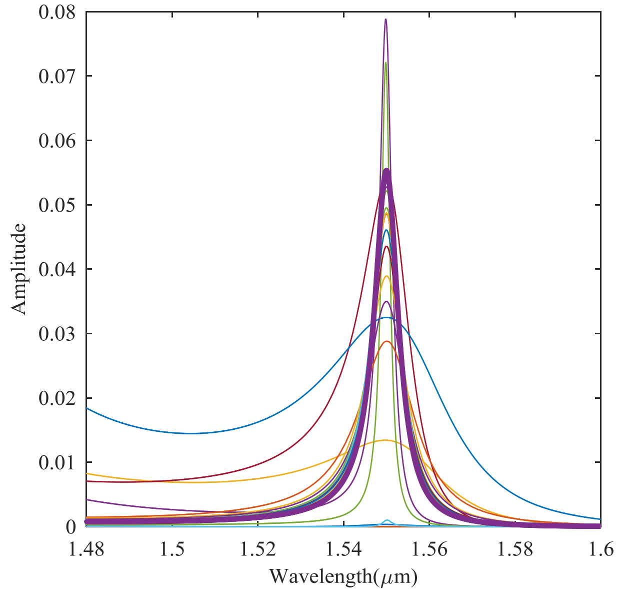

Figure 3- 6: Output spectral transmission performance of the PhC sensor designs of Table 3-1. The purple/thick curve indicates the spectrum at the end of optimization, the best design with singe-objective optimization approach.

3-4-2 Multi-objective optimization approach:

The Ampc, Amps. Deviation, and Sensitivity show a conflicting behavior. Therefore, it means that this problem is intrinsically multi-objective. Since there is no single solution for such problem, solving the problem with just single objective optimization approach, in which the combined result of merit factors is considered, causes to find only a member of the set of optimum solutions.

Since the output of the many designs in the search space does not satisfy the condition of $Amp_{c1}>Amp_{s1}$, second simulation has been bypassed, significantly decreasing the total run time of the optimization.

Finally, the optimization ends up with 100 optimal designs. Since calculating the four merit factors requires two simulations, the second simulation is done to calculate the Sensitivity. Therefore, in order to simplify the plot, the output spectral transmission performance for the first simulation of the optimal designs are depicted in (Figure 3-7). The best and the worst designs with respect to each of the merit factors are shown in (Figure 3-8). As it can be seen, the range of optimal designs is so wide. As it is already mentioned, all of the solution of the Pareto-optimal set are optimal and no one is better than the others. Hence, we need to choose a design in which the best trade-off has been established between the merit factors. To select a design from the set of optimal designs, firstly, we omit the designs in which the Ampc1 of them are very low as they transmit a low portion of optical power. Secondly, we omit the designs in which the ratio=Ampc1/ Amps1 is very low. Designs with a ratio lower than 40 have been omitted. Therefore, 33 optimal designs remain, which are shown in (Table 3-2). The output spectral transmission performance of the first simulation of the remaining 33 designs is depicted in (Figure 3-9) and zoom-in in (Figure 3-10).

Among the optimal designs, the design that provides the highest sensitivity (0.314) is the best choice for liquid sensor application, i.e. structure #1 in (Table 3-2). The output spectral transmission performances of the selected design (i.e. structure #1) and the physical geometry of the device are shown in (Figure 3-11) and (Figure 3-12) respectively. It is also seen that a slight change of filling material refractive index results in a clear shift of output transmission spectrum. In addition, the simulation results for a design of filling the holes with Oil (n=1.45) and water (n=1.33) are shown in (Figure 3-13), and it is observed that a big shift in the output spectral transmission performance is led. The comparison between the designed sensor in this work and the similar works reported, the performance of this work based on the newly defined merit factors is much better than that of the similar works reported [111], [112].

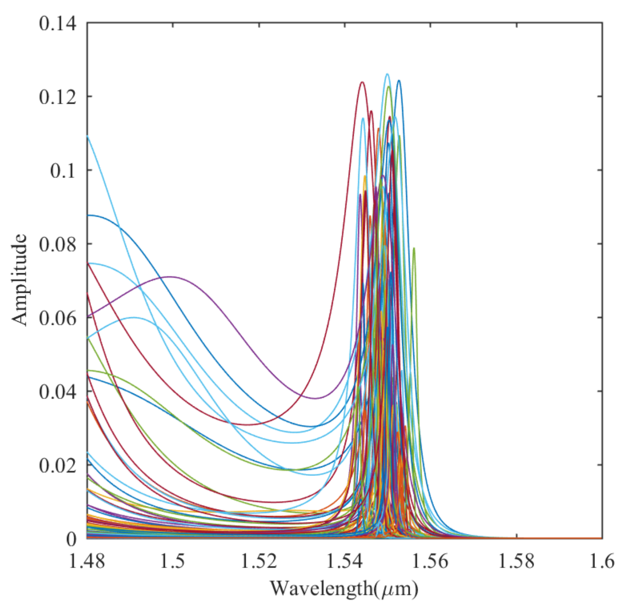

Figure 3- 7: Output spectral transmission performance of the 100 optimal PhC liquid sensor by first simulation.

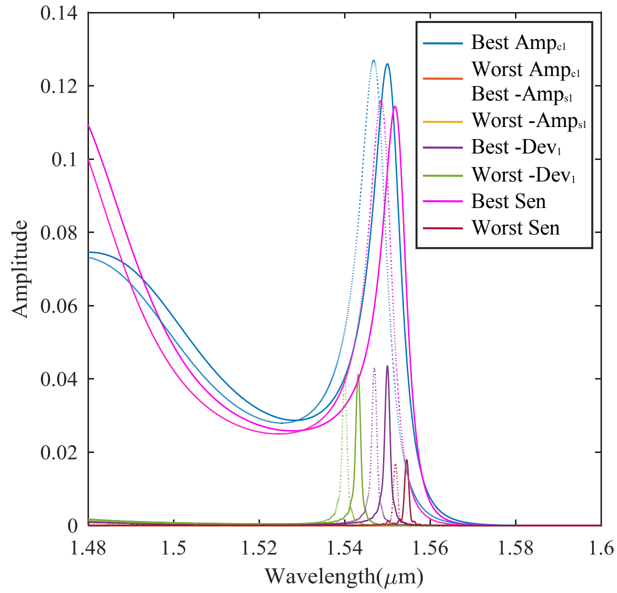

Figure 3- 8: Best and worst designs with respect to each of the merit factors.

Table 3- 2: Properties of optimum structures designed by multi-objective optimization approach.

No.	R_1	R_2	R_3	R_4	R_5	R_6	R_7	R_8	Amp_c	$-Amp_s$	-D(nm)	Sen
1	162	144	98	104	142	138	69	88	0.0756	-0.0017	-2.02	0.314
2	173	149	100	98	141	150	84	98	0.048	-0.0008	-0.75	0.307
3	158	137	105	97	143	148	75	92	0.0756	-0.0016	-0.22	0.307
4	171	156	96	103	137	151	72	84	0.0511	-0.0008	-2.25	0.306
5	174	145	112	94	132	168	89	89	0.0331	-0.0006	-3.07	0.306
6	176	154	102	94	136	163	75	99	0.0305	-0.0004	-4.22	0.301
7	179	157	102	96	131	167	75	99	0.0246	-0.0004	-3.69	0.301
8	167	144	101	94	150	155	79	98	0.0456	-0.0006	-3.39	0.301
9	161	138	103	94	156	159	72	111	0.0526	-0.0006	-1.28	0.3
10	171	135	95	108	141	157	57	72	0.0436	-0.0011	0	0.3
11	151	168	79	112	147	137	76	97	0.0678	-0.0008	-0.53	0.3
12	164	156	93	102	149	142	85	75	0.0537	-0.0008	-1.72	0.299
13	151	151	99	99	151	137	85	82	0.0747	-0.0014	-1.95	0.299
14	178	154	103	95	146	171	72	87	0.0346	-0.0004	-3.67	0.298
15	167	156	93	98	146	152	73	97	0.0451	-0.0005	-5.43	0.294
16	173	143	107	84	158	162	65	82	0.0341	-0.0003	-3.54	0.294
17	177	174	98	91	146	151	81	101	0.0228	-0.0003	-2.86	0.293
18	162	144	97	95	159	167	63	99	0.0289	-0.0003	-2.41	0.293
19	166	152	104	85	164	162	72	107	0.0363	-0.0002	-2.18	0.293
20	173	160	101	94	144	152	74	95	0.0342	-0.0004	-1.05	0.293
21	161	164	80	112	145	140	59	74	0.0567	-0.0008	-0.38	0.292
22	160	157	83	110	148	138	68	84	0.0574	-0.0008	-0.08	0.292
23	159	170	76	116	144	132	73	78	0.0676	-0.001	-0.08	0.292
24	170	153	89	107	147	146	59	88	0.0511	-0.0005	-0.67	0.292
25	174	164	94	96	156	155	65	89	0.0361	-0.0003	-1.43	0.292
26	178	163	108	85	151	162	77	98	0.0212	-0.0002	-1.43	0.292
27	173	164	77	119	139	137	65	84	0.0616	-0.0008	-1.43	0.292
28	181	165	115	80	150	160	61	68	0.0124	-0.0001	-1.58	0.292
29	172	166	97	89	155	169	75	116	0.0193	-0.0002	-3.23	0.286
30	172	163	98	87	164	161	75	83	0.0208	-0.0002	-3.08	0.286
31	195	155	108	81	162	173	55	82	0.0184	-0.0001	-0.23	0.285
32	183	165	94	96	153	163	63	96	0.0305	-0.0002	-1.13	0.284
33	192	184	77	95	179	165	42	103	0.018	-0.0001	-4.52	0.264

The unit of Rx is nm.

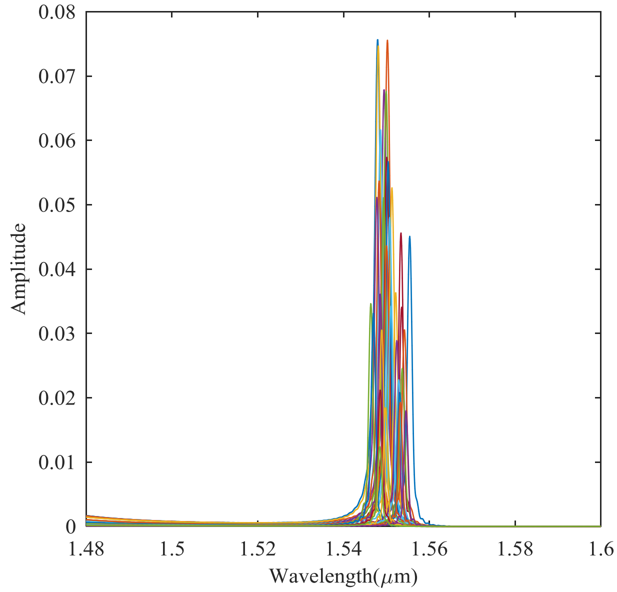

Figure 3- 9: Output spectral transmission performance of the optimal PhC liquid sensors of Table 3-2 by first simulation.

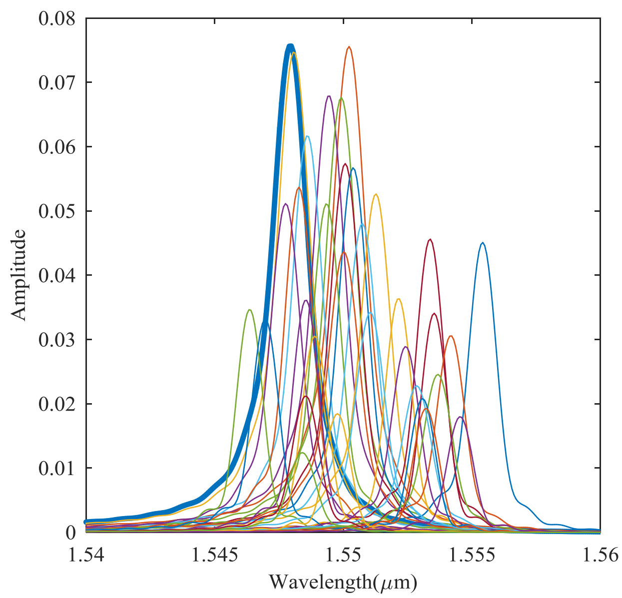

Figure 3- 10: Zoom-in output spectral transmission performance of the optimal PhC liquid sensors of Table 3-2 by first simulation. The thick curve indicates the design has higher sensitivity than the others.

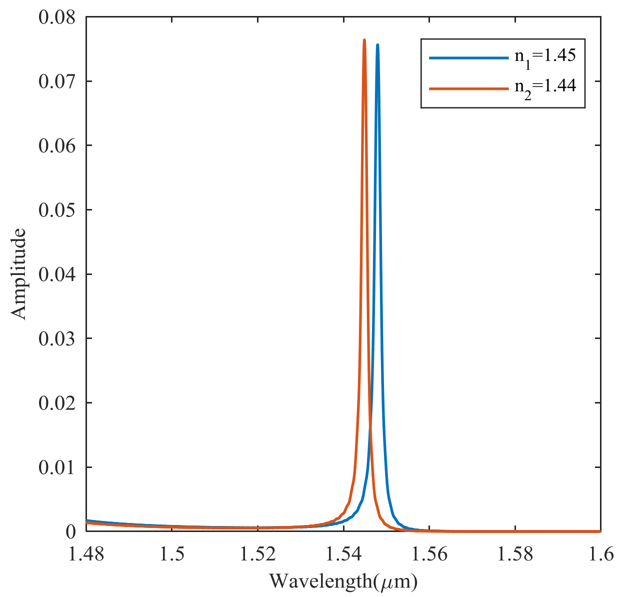

Figure 3- 11: Output spectral transmission performance of the selected optimal PhC liquid sensor by two simulations with different filler materials.

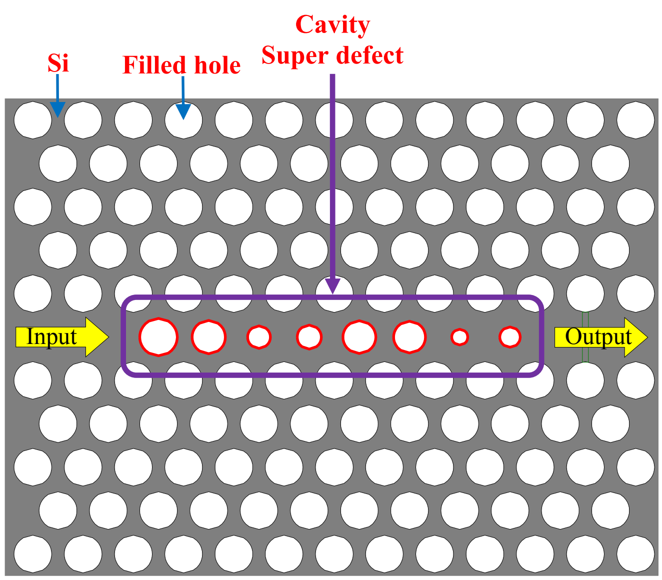

Figure 3- 12: Physical geometry of the obtained PhC liquid sensor.

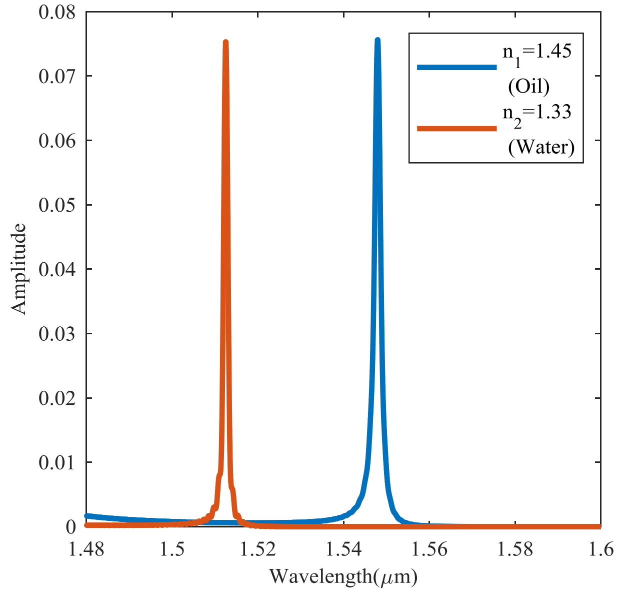

Figure 3- 13: Output spectral transmission performance of the selected optimal PhC liquid sensor in real application.

The method proposed in this study, which is able to automatically find a high-performance design, has two main advantages. First, using a large defect with several free parameters provides much flexibility in manipulating the guided light through the defect. Second, using a systematic multi-objective optimization method allows finding a wide range of optimal designs without human involvement.

To summarize, the multi-objective optimization technique is a straightforward and comprehensive method for designing complex super-defect PhC liquid sensors with a large number of structural parameters. Moreover, this method opens up a way towards designing new and very high-performance PhC Sensors, which work based on the wavelength shift in the output of the PhC filters.

The designed PhC liquid sensor requires 1 nm manufacturing resolution. Considering the fabrication process of PhC structures reported in [141], [142], this structure should be feasible to build.

Chapter 4 Newly proposed Photonic Crystal Sensors

In the previous chapter, a comprehensive method for designing PhC sensor has been proposed [143]. In this chapter we use this method to design new structures of PhC sensor.

4-1 PhC sensor: structure No. 1

In order to increase the flexibility of the PhC sensor, we need to increase the size of the defect section. It provides more control on the transmitted light. The first proposed PhC structure is shown in (Figure 4-1). For this structure 23 holes considered as the defect region. The flexibility of this structure is so high because it has many structural parameters.

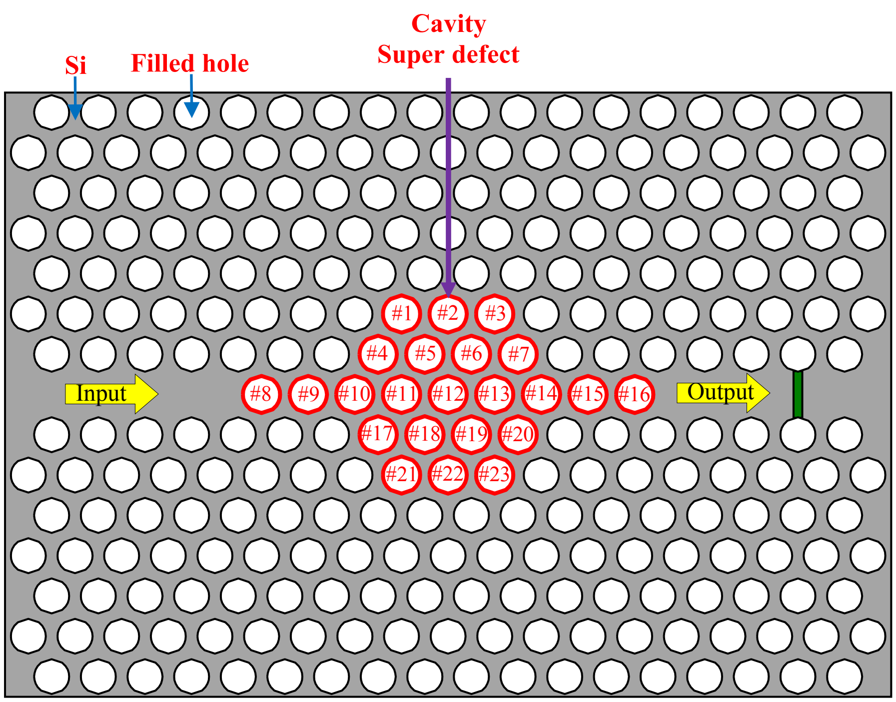

Figure 4- 1: Proposed PhC liquid sensor. 23 holes are used to form the super defect region.

We utilized the method that proposed in the previous chapter. Therefore, for this structure, the optimization ends up with 100 optimal designs. Since calculating the four merit factors requires two simulations, the second simulation is done to calculate the Sensitivity. Therefore, in order to simplify the plot, the output spectral transmission performance for the first simulation of the optimal designs are depicted in (Figure 4-2). As it can be seen, the range of optimal designs is so wide. As it is already mentioned, all of the solution of the Pareto-optimal set are optimal and no one is better than the others. Hence, we need to choose a design in which the best trade-off has been established between the merit factors. To select a design from the set of optimal designs, firstly, we omit the designs in which the Ampc1 of them are very low as they transmit a low portion of optical power. Secondly, we omit the designs in which the ratio=Ampc1/ Amps1 is very low. Designs with a ratio lower than 31 have been omitted. Therefore, 33 optimal designs remain, which are shown in (Table 4-1). The output spectral transmission performance of the first simulation of the remaining 16 designs is depicted in (Figure 4-3) and zoom-in in (Figure 4-4).

Among the optimal designs, the design that provides the highest sensitivity is the best choice for liquid sensor application, i.e. structure #1 in (Table 4-1). The output spectral transmission performances of the selected design (i.e. structure #1) and the physical geometry of the device are shown in (Figure 4-5) and (Figure 4-6) respectively. It is also seen that a slight change of filling material refractive index results in a clear shift of output transmission spectrum. In addition, the simulation results for a design of filling the holes with Oil (n=1.45) and water (n=1.33) are shown in (Figure 4-7), and it is observed that a big shift in the output spectral transmission performance is led.

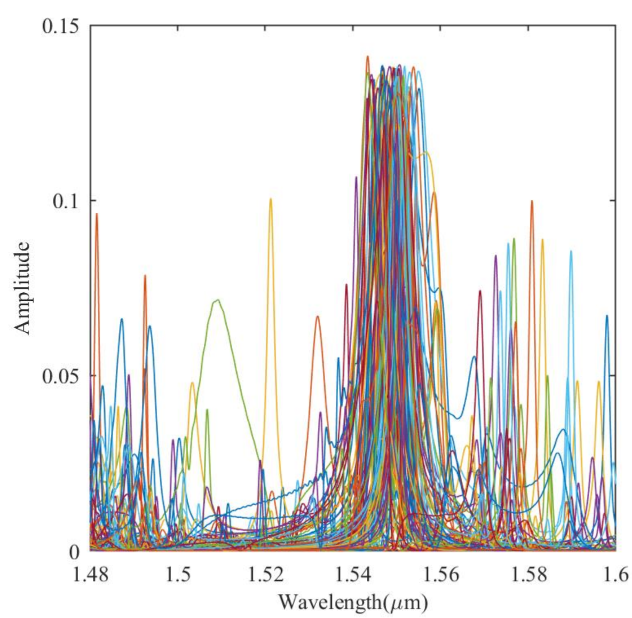

Figure 4- 2: Output spectral transmission performance of the 100 optimal PhC liquid sensor by first simulation.

Table 4- 1: Properties of optimum structures designed by multi-objective optimization approach.

No.	R_1	R_2	R_3	R_4	R_5	R_6	R_7	R_8	R_9	R_{10}	R_{11}	R_{12}	R_{13}	R_{14}	R_{15}	R_{16}	R_{17}	R_{18}	R_{19}	R_{20}	R_{21}	R_{22}	R_{23}	Amp_c	$-Amp_s$	-D(nm)	Sen
1	114	107	158	126	116	109	155	159	150	92	115	40	102	166	162	131	94	137	142	150	106	101	123	0.108	-0.001	-4.118	0.2684
2	91	97	174	104	125	101	157	161	151	83	121	27	113	167	151	153	104	147	146	148	100	110	123	0.0371	-0.0006	-2.997	0.2763
3	96	102	155	131	123	112	153	144	157	120	105	41	115	158	153	137	103	142	128	125	107	110	140	0.1105	-0.0018	-4.442	0.2864
4	101	113	146	122	118	116	139	153	173	98	118	62	93	154	132	141	91	152	116	146	121	106	133	0.1325	-0.0023	-2.482	0.2707
5	96	117	156	108	134	84	133	137	174	108	131	50	125	143	142	132	112	130	141	130	94	129	142	0.13	-0.0024	-3.82	0.2908
6	109	112	152	123	113	84	153	153	143	88	102	51	100	157	143	140	93	134	144	136	108	107	134	0.1216	-0.0025	-2.105	0.2705
7	115	112	151	112	122	88	155	164	153	84	112	51	116	161	128	132	100	134	128	163	94	118	139	0.132	-0.0028	-0.676	0.27
8	111	121	139	129	104	96	135	144	162	103	102	68	101	144	147	129	105	139	119	136	118	112	129	0.1358	-0.003	-1.503	0.2778
9	109	109	153	111	128	73	143	149	150	104	139	48	112	154	132	134	115	147	129	125	120	110	137	0.1239	-0.0027	-0.751	0.2925
10	104	122	135	121	125	97	131	139	156	98	115	49	117	144	144	129	113	130	129	133	113	116	133	0.1371	-0.0031	-0.15	0.2848
11	99	120	160	111	131	78	137	146	164	112	124	51	123	136	137	139	115	140	134	130	98	126	141	0.1346	-0.003	-3.072	0.2986
12	99	112	156	110	139	75	118	152	164	98	129	52	124	144	114	131	125	155	140	131	108	109	140	0.1019	-0.0024	-2.632	0.3007
13	96	124	140	152	109	82	144	128	147	107	118	46	113	145	139	138	95	123	125	140	107	116	140	0.0846	-0.002	-0.225	0.2848
14	89	108	137	127	126	115	129	138	158	109	155	78	91	153	114	116	101	145	139	128	128	92	153	0.0411	-0.0012	-0.825	0.3069
15	101	116	160	110	129	78	134	157	167	115	124	52	121	136	141	142	115	133	143	123	95	125	139	0.1304	-0.0039	-0.3	0.2998
16	121	106	149	122	121	88	150	149	146	107	115	55	115	146	133	131	99	140	133	129	100	119	147	0.1357	-0.0043	-2.324	0.2914

The unit of R_x is *nm*.

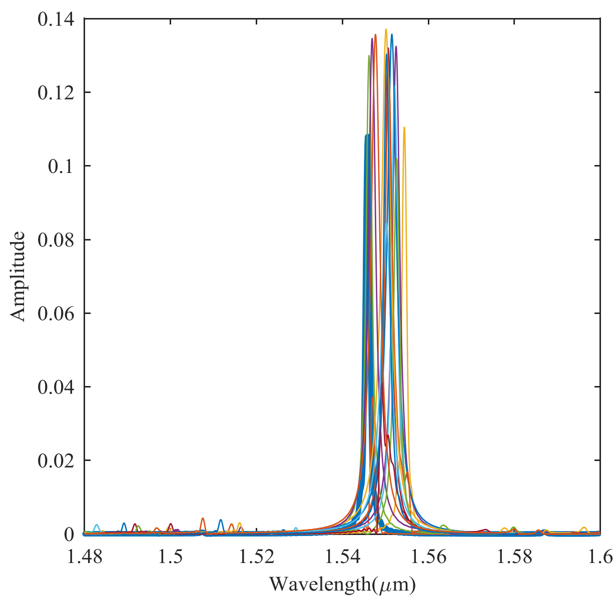

Figure 4- 3: Output spectral transmission performance of the optimal PhC liquid sensors of Table 4-2 by first simulation.

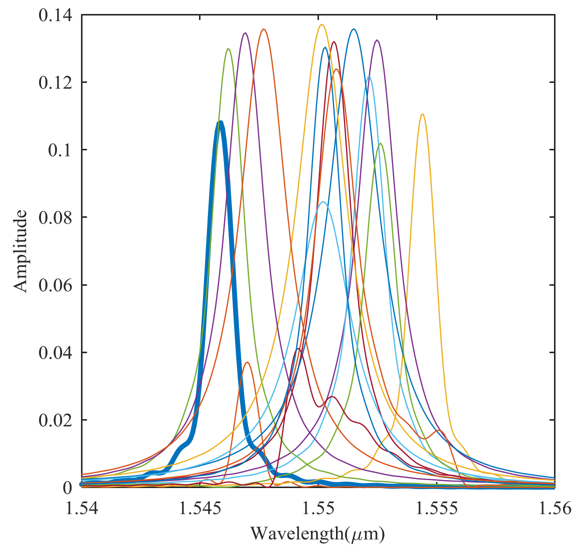

Figure 4- 4: Zoom-in output spectral transmission performance of the optimal PhC liquid sensors of Table 4-1 by first simulation. The thick curve indicates the design has higher sensitivity than the others.

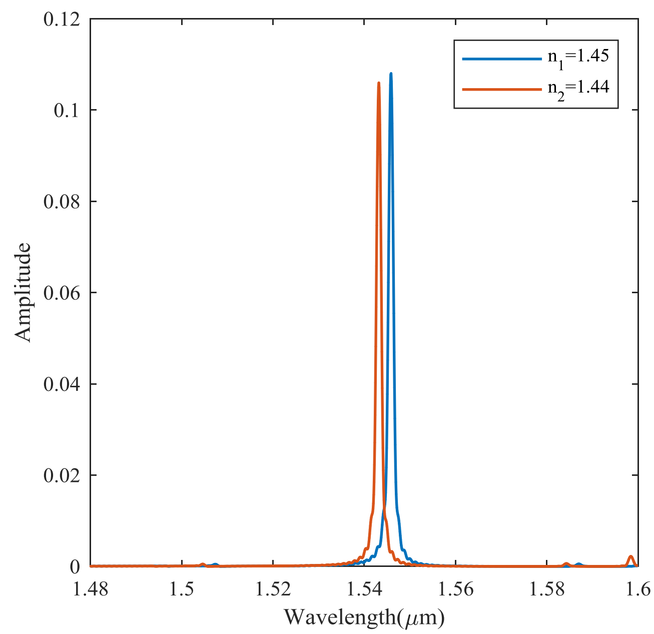

Figure 4- 5: Output spectral transmission performance of the selected optimal PhC liquid sensor by two simulations with different filler materials.

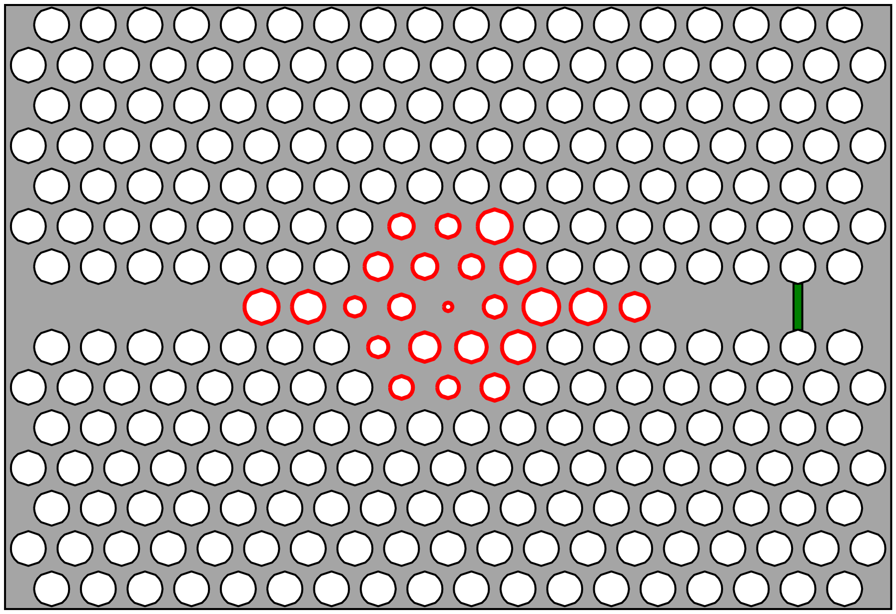

Figure 4- 6: Physical geometry of the obtained PhC liquid sensor.

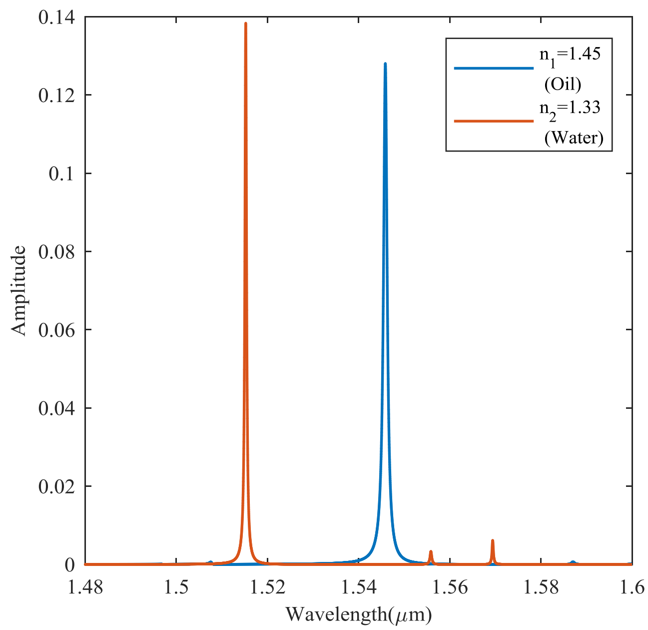

Figure 4- 7: Output spectral transmission performance of the selected optimal PhC liquid sensor in real application.

4-2 PhC sensor: structure No. 2

In order to increase the flexibility of the PhC sensor, we need to increase the size of the defect section. It provides more control over the transmitted light. The second proposed PhC structure is shown in (Figure 4-8). For this structure 21 holes considered as the defect region. The flexibility of this structure is so high because it has many structural parameters. In addition, to reduce the simulation domain and increase the speed of the optimization process, we considered a horizontal symmetry. This symmetry provides an opportunity to simulate just half of the device. As a result, the simulation time decreases.

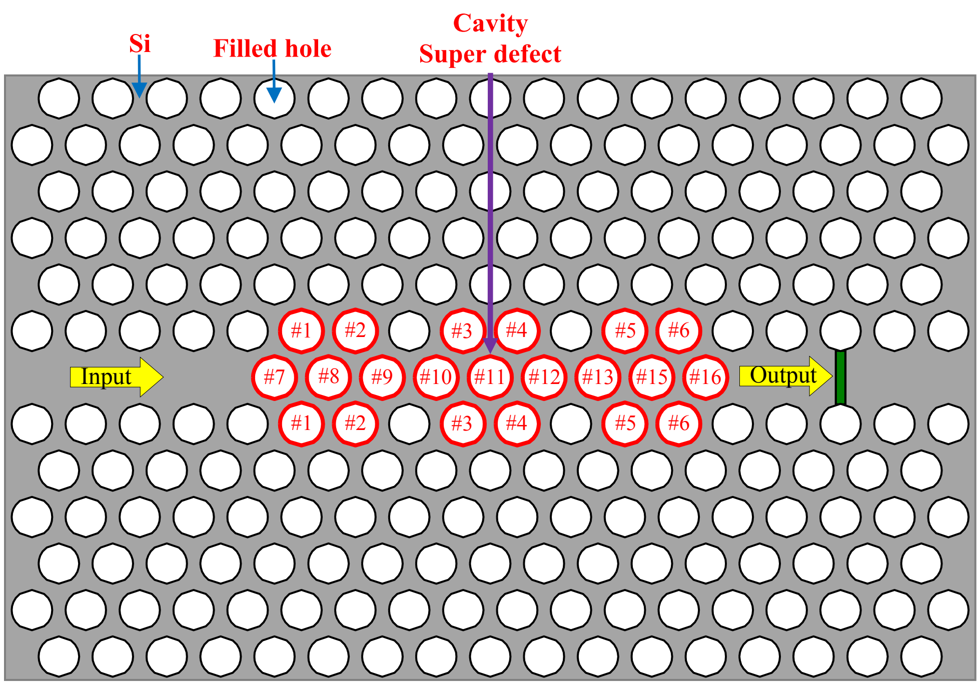

Figure 4- 8: Proposed PhC liquid sensor. 21 holes are used to form the super defect region.

We utilized the method that proposed in the previous chapter. Therefore, for this structure, the optimization ends up with 100 optimal designs. Since calculating the four merit factors requires two simulations, the second simulation is done to calculate the Sensitivity. Therefore, in order to simplify the plot, the output spectral transmission performance for the first simulation of the optimal designs are depicted in (Figure 4-9). As it can be seen, the range of optimal designs is so wide. As it is already mentioned, all of the solution of the Pareto-optimal set are optimal and no one is better than the others. Hence, we need to choose a design in which the best trade-off has been established between the merit factors. To select a design from the set of optimal designs, firstly, we omit the designs in which the Ampc1 of them are very low as they transmit a low portion of optical power. Secondly, we omit the designs in which the ratio=Ampc1/ Amps1 is very low. Designs with a ratio lower than 53 have been omitted. Therefore, 50 optimal designs remain, which are shown in (Table 4-2). The output spectral transmission performance of the first simulation of the remaining 50 designs is depicted in (Figure 4-10) and zoom-in in (Figure 4-11).

Among the optimal designs, the design that provides the highest sensitivity is the best choice for liquid sensor application, i.e. structure #1 in (Table 4-1). The output spectral transmission performances of the selected design (i.e. structure #1) and the physical geometry of the device are shown in (Figure 4-12) and (Figure 4-13) respectively. It is also seen that a slight change of filling material refractive index results in a clear shift of output transmission spectrum. In addition, the simulation results for a design of filling the holes with Oil (n=1.45) and water (n=1.33) are shown in (Figure 4-14), and it is observed that a big shift in the output spectral transmission performance is led.

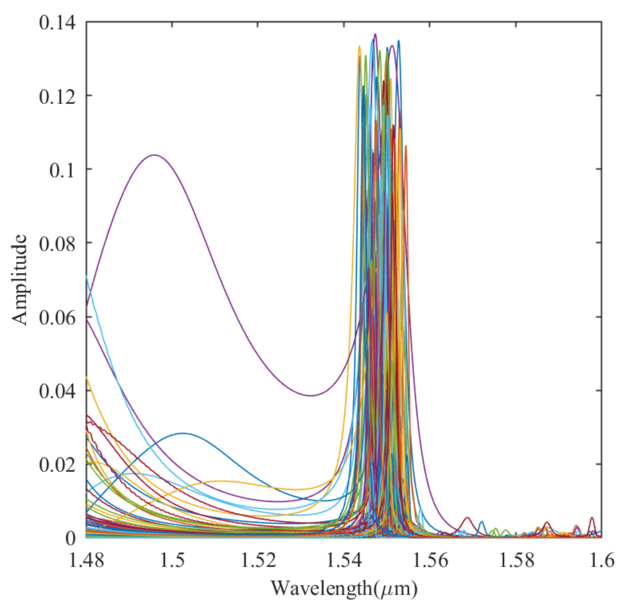

Figure 4- 9: Output spectral transmission performance of the 100 optimal PhC liquid sensor by first simulation.

Table 4- 2: Properties of optimum structures designed by multi-objective optimization approach.

No.	R_1	R_2	R_3	R_4	R_5	R_6	R_7	R_8	R_9	R_{10}	R_{11}	R_{12}	R_{13}	R_{14}	R_{15}	Amp_c	$-Amp_s$	-D(nm)	Sen
1	135	144	154	65	178	144	104	156	156	75	184	86	124	128	152	0.0742	-0.0012	-2.698	0.3285
2	102	144	153	71	166	139	108	181	135	84	181	124	122	124	162	0.0262	-0.0002	-1.725	0.3284
3	116	148	165	68	168	139	105	192	133	78	184	107	124	123	162	0.0606	-0.0003	-3.222	0.3282
4	117	142	157	64	170	123	114	178	147	76	187	110	126	156	163	0.0197	-0.0001	-3.595	0.3282
5	156	134	175	54	171	126	100	184	129	83	181	65	118	163	157	0.0555	-0.0002	-0.45	0.322
6	123	147	154	69	161	140	98	172	141	87	173	86	137	130	148	0.0978	-0.0013	-1.425	0.3216
7	124	137	149	81	146	141	98	174	137	94	162	103	136	126	157	0.1173	-0.002	-3.894	0.3206
8	127	145	166	58	165	141	102	169	139	92	171	78	143	134	164	0.0732	-0.0007	-4.268	0.3204
9	130	140	143	78	145	150	96	167	136	91	169	104	133	124	154	0.1065	-0.0019	-4.367	0.3165
10	138	149	164	58	164	146	92	174	145	80	175	77	138	133	167	0.0637	-0.0005	-2.406	0.3156
11	150	137	154	69	152	155	93	166	138	95	162	74	148	120	156	0.1083	-0.0016	-1.955	0.3155
12	123	172	160	54	177	119	124	177	152	75	180	107	154	156	154	0.0133	0	-0.675	0.3145
13	122	149	141	77	171	124	97	169	144	86	174	93	142	143	149	0.0876	-0.0006	-1.875	0.3139
14	144	143	143	81	155	144	95	158	142	99	156	88	141	132	149	0.1134	-0.0018	-2.623	0.3137
15	129	146	152	69	158	140	102	170	154	79	175	99	144	141	151	0.0856	-0.0005	-3.072	0.3135
16	127	140	161	71	155	141	101	172	145	83	168	91	145	129	150	0.1045	-0.0011	-3.222	0.3134
17	93	156	163	54	179	115	120	183	146	72	185	123	130	164	171	0.0058	0	-4.216	0.3089
18	140	136	161	70	161	141	103	167	138	89	160	79	134	134	159	0.0891	-0.0009	-3.763	0.3087
19	115	156	168	46	183	140	113	193	151	62	190	109	165	153	172	0.0062	0	-3.461	0.3086
20	124	140	150	75	155	132	112	157	137	94	162	95	143	135	140	0.1159	-0.0022	-2.934	0.3084
21	117	156	150	65	165	119	112	183	152	82	172	111	144	147	152	0.0403	-0.0001	0	0.3072
22	126	156	148	69	160	119	118	155	154	86	170	101	151	148	153	0.0782	-0.0004	-2.698	0.3062
23	137	140	147	83	163	136	80	169	140	93	153	79	133	140	151	0.0989	-0.0014	-2.482	0.3007
24	140	151	144	73	171	151	92	163	148	95	157	77	149	136	148	0.0866	-0.0005	-1.428	0.3003
25	143	140	148	77	155	145	95	156	151	94	151	92	147	130	155	0.1179	-0.0013	0	0.2997
26	147	140	148	76	157	138	102	161	145	96	155	97	140	135	154	0.1096	-0.0008	-0.9	0.2994
27	94	169	159	46	186	137	130	175	164	78	171	111	169	165	161	0.0007	0	-7.165	0.2949
28	158	150	164	53	165	149	107	156	148	93	160	94	144	141	174	0.0433	-0.0001	-3.763	0.2937
29	136	149	145	74	166	151	96	164	148	94	157	84	147	135	153	0.0862	-0.0004	-1.653	0.2928
30	125	151	165	66	167	117	106	181	149	73	169	85	145	139	163	0.0529	-0.0002	-0.901	0.2925
31	147	139	148	73	163	84	101	170	147	79	159	110	146	141	158	0.0483	-0.0006	0	0.2923
32	122	166	161	49	178	112	122	152	162	81	173	101	175	146	162	0.0322	-0.0001	-0.825	0.292
33	124	154	126	82	153	133	99	155	161	91	161	106	148	132	164	0.0996	-0.0006	-1.277	0.2852
34	123	159	165	52	168	128	106	172	161	79	168	93	158	155	160	0.0379	-0.0001	-0.375	0.2849
35	141	171	165	48	175	123	134	174	161	81	170	94	165	164	159	0.0067	0	-1.425	0.2843
36	128	154	164	54	177	123	121	170	146	101	152	88	156	153	165	0.026	-0.0001	-0.15	0.2773
37	140	173	161	54	177	120	122	163	162	76	165	86	166	145	160	0.0159	0	-3.763	0.2711
38	118	157	157	56	175	123	121	160	152	84	173	102	164	150	158	0.0452	-0.0001	-0.15	0.2698
39	126	167	150	62	168	121	131	162	165	81	168	91	171	146	158	0.0206	-0.0001	-1.65	0.2692
40	130	143	161	62	182	144	93	158	164	88	143	83	156	136	175	0.0664	-0.0002	-2.482	0.2632
41	134	147	158	58	179	141	89	176	174	66	169	73	170	148	171	0.048	-0.0001	-2.18	0.263
42	126	152	142	76	178	124	98	164	155	80	159	93	154	148	152	0.082	-0.0003	0	0.2623
43	132	168	149	59	166	115	139	147	168	74	177	108	158	151	155	0.0175	0	-2.256	0.2556
44	141	162	173	45	183	136	116	175	176	67	167	89	168	152	163	0.0183	-0.0001	-0.975	0.2546
45	154	159	164	54	170	134	91	156	157	92	144	92	159	158	175	0.0538	-0.0002	-4.065	0.2487
46	120	159	157	53	179	140	113	173	158	83	168	106	160	157	159	0.0228	0	-1.052	0.2477
47	155	162	156	57	164	150	106	157	148	98	147	104	163	157	184	0.0325	-0.0001	-0.451	0.2475
48	153	168	154	64	175	145	95	164	171	74	147	80	171	151	180	0.0287	-0.0001	-2.934	0.2408
49	116	186	157	45	187	127	143	176	171	65	180	98	188	161	162	0.0002	0	-0.3	0.2324
50	152	168	177	39	182	141	99	170	170	71	150	102	173	172	190	0.0148	0	-0.15	0.2174

The unit of R_x is *nm*.

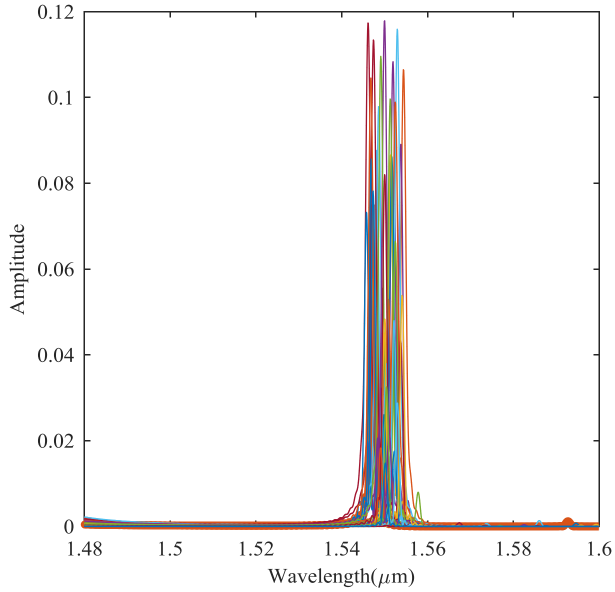

Figure 4- 10: Output spectral transmission performance of the optimal PhC liquid sensors of Table 4-2 by first simulation.

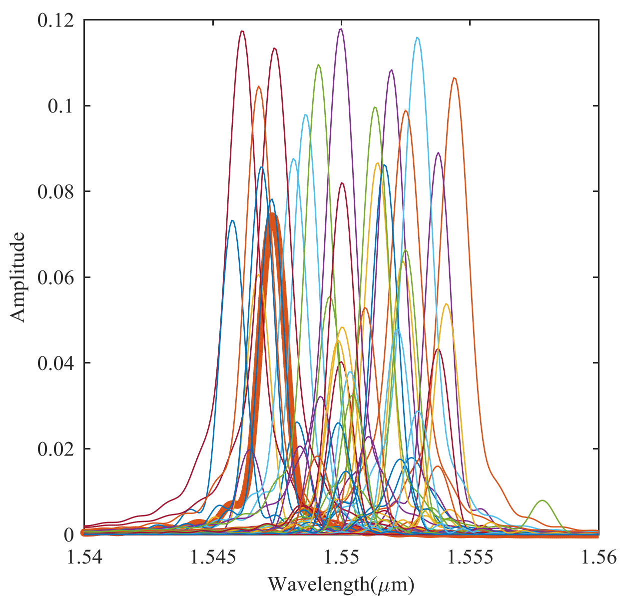

Figure 4- 11: Zoom-in output spectral transmission performance of the optimal PhC liquid sensors of Table 4-2 by first simulation. The thick curve indicates the design has higher sensitivity than the others.

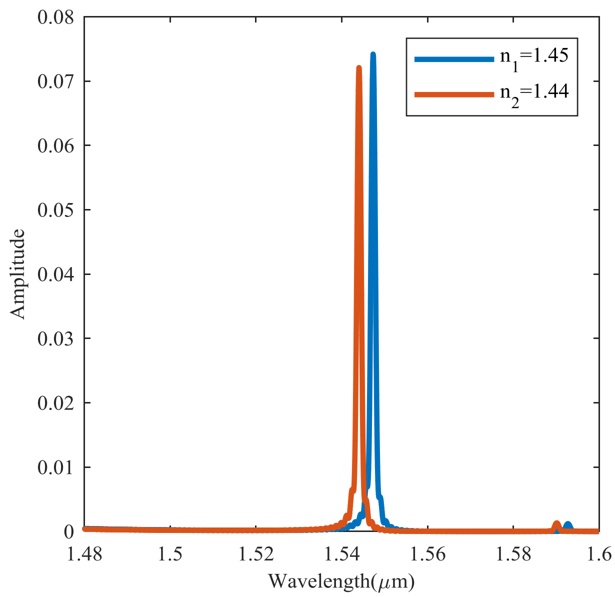

Figure 4- 12: Output spectral transmission performance of the selected optimal PhC liquid sensor by two simulations with different filler materials.

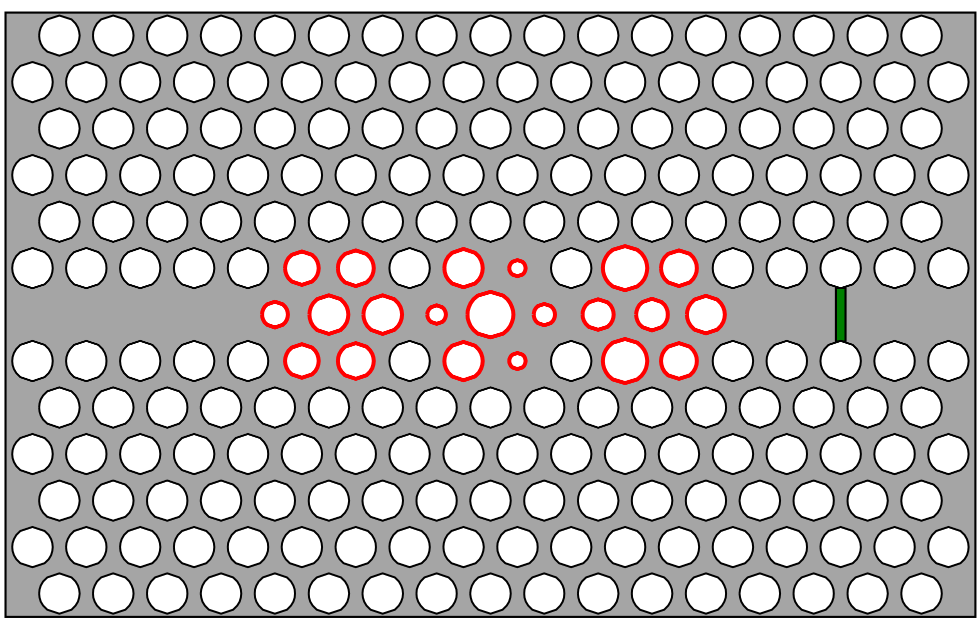

Figure 4- 13: Physical geometry of the obtained PhC liquid sensor.

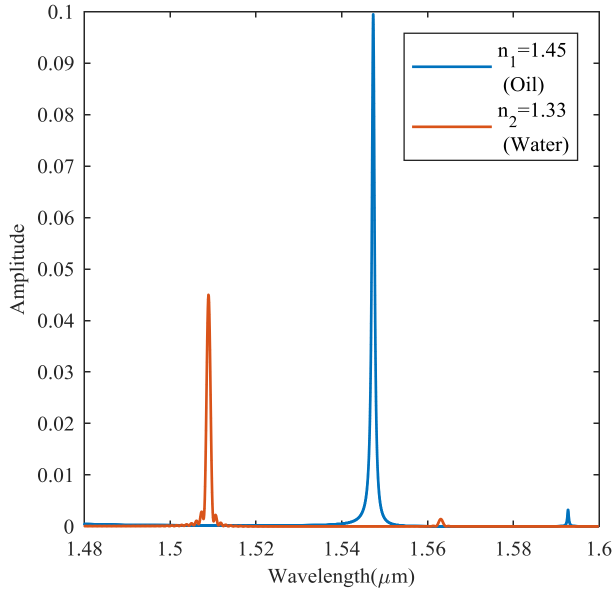

Figure 4- 14: Output spectral transmission performance of the selected optimal PhC liquid sensor in real application.

Chapter5 Conclusion and potential future work

In summary, the case study investigated here has shown that the proposed multi-objective framework can effectively design and optimize the structure of a newly introduced PhC liquid sensor. The proposed framework can design any complicated super-defect PhC sensors. Several structures can be designed with respect to any application. No initial design and human involvement are required to start the optimization process. Moreover, any manufacturing limitation can be added in the constraints module. Various multi-objective algorithms can be easily used in optimizer module to achieve the optimal designs. Finally, the proposed multi-objective framework opens up an effective way for designing very high-performance PhC sensors.

Potential future work:

- Propose a method for considering fabrication uncertainties during the optimization of PhC sensors.
- Utilizing the proposed framework for designing different kind of PhC sensors.
- Investigate the applicability of the optimized structures in configuration with photonic integrated circuits.

References

[1] K. M. Ho, C. T. Chan, C. M. Soukoulis, R. Biswas, and M. Sigalas, “Photonic band gaps in three dimensions: New layer-by-layer periodic structures,” *Solid State Commun.*, vol. 89, no. 5, pp. 413–416, 1994.

[2] E. Yablonovitch, “Inhibited spontaneous emission in solid-state physics and electronics,” *Phys. Rev. Lett.*, vol. 58, no. 20, pp. 2059–2062, 1987.

[3] S. John, “Strong localization of photons in certain disordered dielectric superlattices,” *Phys. Rev. Lett.*, vol. 58, no. 23, pp. 2486–2489, 1987.

[4] Lord Rayleigh, “XXVI. On the remarkable phenomenon of crystalline reflexion described by Prof. Stokes,” *London, Edinburgh, Dublin Philos. Mag. J. Sci.*, vol. 26, no. 160, pp. 256–265, 1888.

[5] V. P. Bykov, “Spontaneous emission in a periodic structure,” *Sov. J. Exp. Theor. Phys.*, vol. 35, p. 269, 1972.

[6] S. Lin, J. G. Fleming, D. L. Hetherington, B. K. Smith, R. Biswas, K. M. Ho, M. M. Sigalas, W. Zubrzycki, S. R. Kurtz, and J. Bur, “A three-dimensional photonic crystal operating at infrared wavelengths,” *Nature*, vol. 394, no. 6690, p. 251, 1998.

[7] V. P. Bykov, “Spontaneous emission from a medium with a band spectrum,” *Sov. J. Quantum Electron.*, vol. 4, no. 7, p. 861, 1975.

[8] K. Ohtaka, “Energy band of photons and low-energy photon diffraction,” *Phys. Rev. B*, vol. 19, no. 10, p. 5057, 1979.

[9] P. Viktorovitch, E. Drouard, M. Garrigues, J. L. Leclercq, X. Letartre, P. R. Romeo, and C. Seassal, “Photonic crystals: basic concepts and devices,” *Comptes Rendus Phys.*, vol. 8, no. 2, pp. 253–266, 2007.

[10] J. D. Joannopoulos, S. G. Johnson, J. N. Winn, and R. D. Meade, *Photonic crystals: molding the flow of light*. Princeton university press, 2011.

[11] J. D. Joannopoulos, P. R. Villeneuve, and S. Fan, “Photonic crystals: putting a new twist on light,” *Nature*, vol. 386, no. 6621, p. 143, 1997.

[12] A. Scherer, O. Painter, J. Vuckovic, M. Loncar, and T. Yoshie, “Photonic crystals for confining, guiding, and emitting light,” *IEEE Trans. Nanotechnol.*, vol. 99, no. 1, pp. 4–11, 2002.

[13] K. Fasihi, “High-contrast all-optical controllable switching and routing in nonlinear photonic crystals,” *J. Light. Technol.*, vol. 32, no. 18, pp. 3126–3131, 2014.

[14] J. O’Brien and W. Kuang, “Photonic Crystal Lasers, Cavities and Waveguides,” 2018.

[15] T. Tanabe, M. Notomi, S. Mitsugi, A. Shinya, and E. Kuramochi, “All-optical switches on a silicon chip realized using photonic crystal nanocavities,” *Appl. Phys. Lett.*, vol. 87, no. 15, p. 151112, 2005.

[16] T. Baba, “Slow light in photonic crystals,” *Nat. Photonics*, vol. 2, no. 8, p. 465, 2008.

[17] Y. Zhao, Y.-N. Zhang, and Q. Wang, “Research advances of photonic crystal gas and liquid sensors,” *Sensors Actuators B Chem.*, vol. 160, no. 1, pp. 1288–1297, 2011.

[18] W.-C. Lai, S. Chakravarty, X. Wang, C. Lin, and R. T. Chen, “On-chip methane sensing by near-IR absorption signatures in a photonic crystal slot waveguide,” *Opt. Lett.*, vol. 36, no. 6, pp. 984–986, 2011.

[19] Y. Zhang, Y. Zhao, and Q. Wang, “Multi-component gas sensing based on slotted photonic crystal waveguide with liquid infiltration,” *Sensors Actuators B Chem.*, vol. 184, pp. 179–188, 2013.

[20] Y. Zhang, Y. Zhao, and Q. Wang, “Measurement of methane concentration with cryptophane E infiltrated photonic crystal microcavity,” *Sensors Actuators B Chem.*, vol. 209, pp. 431–437, 2015.
[21] Y.-H. Chang, Y.-Y. Jhu, and C.-J. Wu, “Temperature dependence of defect mode in a defective photonic crystal,” *Opt. Commun.*, vol. 285, no. 6, pp. 1501–1504, 2012.
[22] E. Chow, A. Grot, L. W. Mirkarimi, M. Sigalas, and G. Girolami, “Ultracompact biochemical sensor built with two-dimensional photonic crystal microcavity,” *Opt. Lett.*, vol. 29, no. 10, pp. 1093–1095, 2004.
[23] Y. Liu and H. W. M. Salemink, “All-optical on-chip sensor for high refractive index sensing in photonic crystals,” *EPL (Europhysics Lett.*, vol. 107, no. 3, p. 34008, 2014.
[24] S. Zheng, B. Shan, M. Ghandehari, and J. Ou, “Sensitivity characterization of cladding modes in long-period gratings photonic crystal fiber for structural health monitoring,” *Measurement*, vol. 72, pp. 43–51, 2015.
[25] A. Casas-Bedoya, S. Shahnia, D. Di Battista, E. Mägi, and B. J. Eggleton, “Chip scale humidity sensing based on a microfluidic infiltrated photonic crystal,” *Appl. Phys. Lett.*, vol. 103, no. 18, p. 181109, 2013.
[26] S. Zheng, Y. Zhu, and S. Krishnaswamy, “Fiber humidity sensors with high sensitivity and selectivity based on interior nanofilm-coated photonic crystal fiber long-period gratings,” *Sensors Actuators B Chem.*, vol. 176, pp. 264–274, 2013.
[27] S. Zheng, Y. Zhu, and S. Krishnaswamy, “Nanofilm-coated photonic crystal fiber long-period gratings with modal transition for high chemical sensitivity and selectivity,” in *Smart Sensor Phenomena, Technology, Networks, and Systems Integration 2012*, 2012, vol. 8346, p. 83460D.
[28] C.-Y. Lin, H. Subbaraman, A. Hosseini, A. X. Wang, L. Zhu, and R. T. Chen, “Silicon nanomembrane based photonic crystal waveguide array for wavelength-tunable true-time-delay lines,” *Appl. Phys. Lett.*, vol. 101, no. 5, p. 51101, 2012.
[29] A. Sopaheluwakan, “Defect states and defect modes in 1D photonic crystals,” *MSc. Univ. Twente, Netherlands*, 2003.
[30] C. Fenzl, T. Hirsch, and O. S. Wolfbeis, “Photonic crystals for chemical sensing and biosensing,” *Angew. Chemie Int. Ed.*, vol. 53, no. 13, pp. 3318–3335, 2014.
[31] B. Li and C. Lee, “NEMS diaphragm sensors integrated with triple-nano-ring resonator,” *Sensors Actuators A Phys.*, vol. 172, no. 1, pp. 61–68, 2011.
[32] D. Wang, Z. Yu, Y. Liu, X. Guo, C. Shu, S. Zhou, and J. Zhang, “Ultrasmall modal volume and high Q factor optimization of a photonic crystal slab cavity,” *J. Opt.*, vol. 15, no. 12, p. 125102, 2013.
[33] Y. Akahane, T. Asano, B.-S. Song, and S. Noda, “High-Q photonic nanocavity in a two-dimensional photonic crystal,” *Nature*, vol. 425, no. 6961, p. 944, 2003.
[34] Y. Zhang, D. Li, C. Zeng, Z. Huang, Y. Wang, Q. Huang, Y. Wu, J. Yu, and J. Xia, “Silicon optical diode based on cascaded photonic crystal cavities,” *Opt. Lett.*, vol. 39, no. 6, pp. 1370–1373, 2014.
[35] A. Majumdar, J. Kim, J. Vuckovic, and F. Wang, “Electrical control of silicon photonic crystal cavity by graphene,” *Nano Lett.*, vol. 13, no. 2, pp. 515–518, 2013.
[36] C. Caër, X. Le Roux, and E. Cassan, “High-Q silicon-on-insulator slot photonic crystal cavity infiltrated by a liquid,” *Appl. Phys. Lett.*, vol. 103, no. 25, p. 251106, 2013.
[37] D. Yang, H. Tian, and Y. Ji, “Nanoscale low crosstalk photonic crystal integrated sensor array,” *IEEE Photonics J.*, vol. 6, no. 1, pp. 1–7, 2014.

[38] Y.-J. Fu, Y.-S. Lee, and S.-D. Lin, “Design and demonstration of high quality-factor H1-cavity in two-dimensional photonic crystal,” *Opt. Lett.*, vol. 38, no. 22, pp. 4915–4918, 2013.
[39] Y. Yang, D. Yang, H. Tian, and Y. Ji, “Photonic crystal stress sensor with high sensitivity in double directions based on shoulder-coupled aslant nanocavity,” *Sensors Actuators A Phys.*, vol. 193, pp. 149–154, 2013.
[40] Y.-N. Zhang, Y. Zhao, D. Wu, and Q. Wang, “Fiber Loop Ring-Down Refractive Index Sensor Based on High-$ Q $ Photonic Crystal Cavity,” *IEEE Sens. J.*, vol. 14, no. 6, pp. 1878–1885, 2014.
[41] A. F. Oskooi, D. Roundy, M. Ibanescu, P. Bermel, J. D. Joannopoulos, and S. G. Johnson, “MEEP: A flexible free-software package for electromagnetic simulations by the FDTD method,” *Comput. Phys. Commun.*, vol. 181, no. 3, pp. 687–702, 2010.
[42] A. C. S Jr, K. Z. Nobrega, H. E. Hernandez-Figueroa, and F. Di Pasquale, “PCFDT: An accurate and friendly photonic crystal fiber design tool,” *Opt. J. Light Electron Opt.*, vol. 119, no. 15, pp. 723–732, 2008.
[43] Q. Yan, Z. Zhou, and X. S. Zhao, “Inward-growing self-assembly of colloidal crystal films on horizontal substrates,” *Langmuir*, vol. 21, no. 7, pp. 3158–3164, 2005.
[44] V. Berger, O. Gauthier-Lafaye, and E. Costard, “Photonic band gaps and holography,” *J. Appl. Phys.*, vol. 82, no. 1, pp. 60–64, 1997.
[45] M. Campbell, D. N. Sharp, M. T. Harrison, R. G. Denning, and A. J. Turberfield, “Fabrication of photonic crystals for the visible spectrum by holographic lithography,” *Nature*, vol. 404, no. 6773, p. 53, 2000.
[46] O. D. Velev, T. A. Jede, R. F. Lobo, and A. M. Lenhoff, “Porous silica via colloidal crystallization,” *Nature*, vol. 389, no. 6650, p. 447, 1997.
[47] A. A. Zakhidov, R. H. Baughman, Z. Iqbal, C. Cui, I. Khayrullin, S. O. Dantas, J. Marti, and V. G. Ralchenko, “Carbon structures with three-dimensional periodicity at optical wavelengths,” *Science (80-.).*, vol. 282, no. 5390, pp. 897–901, 1998.
[48] A. Blanco, E. Chomski, S. Grabtchak, M. Ibisate, S. John, S. W. Leonard, C. Lopez, F. Meseguer, H. Miguez, and J. P. Mondia, “Large-scale synthesis of a silicon photonic crystal with a complete three-dimensional bandgap near 1.5 micrometres,” *Nature*, vol. 405, no. 6785, p. 437, 2000.
[49] V. N. Astratov, Y. A. Vlasov, O. Z. Karimov, A. A. Kaplyanskii, Y. G. Musikhin, N. A. Bert, V. N. Bogomolov, and A. V Prokofiev, “Photonic band gaps in 3D ordered fcc silica matrices,” *Phys. Lett. A*, vol. 222, no. 5, pp. 349–353, 1996.
[50] R. Mayoral, J. Requena, J. S. Moya, C. López, A. Cintas, H. Miguez, F. Meseguer, L. Vázquez, M. Holgado, and Á. Blanco, “3D Long-range ordering in ein SiO2 submicrometer-sphere sintered superstructure,” *Adv. Mater.*, vol. 9, no. 3, pp. 257–260, 1997.
[51] P. Jiang, J. F. Bertone, K. S. Hwang, and V. L. Colvin, “Single-crystal colloidal multilayers of controlled thickness,” *Chem. Mater.*, vol. 11, no. 8, pp. 2132–2140, 1999.
[52] J. Vučković, M. Lončar, H. Mabuchi, and A. Scherer, “Design of photonic crystal microcavities for cavity QED,” *Phys. Rev. E*, vol. 65, no. 1, p. 16608, 2001.
[53] T. Tanabe, M. Notomi, E. Kuramochi, A. Shinya, and H. Taniyama, “Trapping and delaying photons for one nanosecond in an ultrasmall high-Q photonic-crystal nanocavity,” *Nat. Photonics*, vol. 1, no. 1, p. 49, 2007.
[54] T. Sünner, M. Gellner, A. Löffler, M. Kamp, and A. Forchel, “Group delay measurements

on photonic crystal resonators," *Appl. Phys. Lett.*, vol. 90, no. 15, p. 151117, 2007.
[55] J. Hodgkinson and R. P. Tatam, "Optical gas sensing: a review," *Meas. Sci. Technol.*, vol. 24, no. 1, p. 12004, 2012.
[56] W. R. Seitz, "Chemical sensors based on fiber optics," *Anal. Chem.*, vol. 56, no. 1, p. 16A–34A, 1984.
[57] H. Awad, I. Hasan, K. Mnaymneh, T. J. Hall, and I. Andonovic, "Gas sensing using slow light in photonic crystal waveguides," in *Fibre and Optical Passive Components (WFOPC), 2011 7th Workshop on*, 2011, pp. 1–3.
[58] Y. Zhao, Y. Zhang, and Q. Wang, "High sensitivity gas sensing method based on slow light in photonic crystal waveguide," *Sensors Actuators B Chem.*, vol. 173, pp. 28–31, 2012.
[59] A. Kumar, T. S. Saini, and R. K. Sinha, "Design and analysis of photonic crystal biperiodic waveguide structure based optofluidic-gas sensor," *Opt. J. Light Electron Opt.*, vol. 126, no. 24, pp. 5172–5175, 2015.
[60] A. K. Goyal, H. S. Dutta, and S. Pal, "Recent advances and progress in photonic crystal-based gas sensors," *J. Phys. D. Appl. Phys.*, vol. 50, no. 20, p. 203001, 2017.
[61] D. Benelarbi, T. Bouchemat, and M. Bouchemat, "Design of high-sensitive refractive index sensor using a ring-shaped photonic crystal waveguide," *Nanosci. Nanotechnol.*, vol. 6, no. 1A, pp. 105–109, 2016.
[62] A. Di Falco, L. O'Faolain, and T. F. Krauss, "Photonic crystal slotted slab waveguides," *Photonics Nanostructures-Fundamentals Appl.*, vol. 6, no. 1, pp. 38–41, 2008.
[63] A. Di Falco, L. O'Faolain, and T. F. Krauss, "Dispersion control and slow light in slotted photonic crystal waveguides," *Appl. Phys. Lett.*, vol. 92, no. 8, p. 83501, 2008.
[64] H. Aghababaeian, M.-H. Vadjed-Samiei, and N. Granpayeh, "Temperature stabilization of group index in silicon slotted photonic crystal waveguides," *J. Opt. Soc. Korea*, vol. 15, no. 4, pp. 398–402, 2011.
[65] R. K. Gangwar and V. K. Singh, "Refractive index sensor based on selectively liquid infiltrated dual core photonic crystal fibers," *Photonics Nanostructures-Fundamentals Appl.*, vol. 15, pp. 46–52, 2015.
[66] A. K. Goyal and S. Pal, "Design and simulation of high sensitive photonic crystal waveguide sensor," *Opt. J. Light Electron Opt.*, vol. 126, no. 2, pp. 240–243, 2015.
[67] X. Wang, Z. Xu, N. Lu, J. Zhu, and G. Jin, "Ultracompact refractive index sensor based on microcavity in the sandwiched photonic crystal waveguide structure," *Opt. Commun.*, vol. 281, no. 6, pp. 1725–1731, 2008.
[68] D. F. Dorfner, T. Hürlimann, T. Zabel, L. H. Frandsen, G. Abstreiter, and J. J. Finley, "Silicon photonic crystal nanostructures for refractive index sensing," *Appl. Phys. Lett.*, vol. 93, no. 18, p. 181103, 2008.
[69] L. A. Shiramin, R. Kheradmand, and A. Abbasi, "High-sensitive double-hole defect refractive index sensor based on 2-D photonic crystal," *IEEE Sens. J.*, vol. 13, no. 5, pp. 1483–1486, 2013.
[70] J. Zhou, H. Tian, D. Yang, Q. Liu, and Y. Ji, "Integration of high transmittance photonic crystal H2 nanocavity and broadband W1 waveguide for biosensing applications based on Silicon-on-Insulator substrate," *Opt. Commun.*, vol. 330, pp. 175–183, 2014.
[71] L. Huang, H. Tian, D. Yang, J. Zhou, Q. Liu, P. Zhang, and Y. Ji, "Optimization of figure of merit in label-free biochemical sensors by designing a ring defect coupled resonator," *Opt. Commun.*, vol. 332, pp. 42–49, 2014.

[72] C. Caer, X. Le Roux, and E. Cassan, “Enhanced localization of light in slow wave slot photonic crystal waveguides,” *Opt. Lett.*, vol. 37, no. 17, pp. 3660–3662, 2012.
[73] V. R. Almeida, Q. Xu, C. A. Barrios, and M. Lipson, “Guiding and confining light in void nanostructure,” *Opt. Lett.*, vol. 29, no. 11, pp. 1209–1211, 2004.
[74] T. Yamamoto, M. Notomi, H. Taniyama, E. Kuramochi, Y. Yoshikawa, Y. Torii, and T. Kuga, “Design of a high-Q air-slot cavity based on a width-modulated line-defect in a photonic crystal slab,” *Opt. Express*, vol. 16, no. 18, pp. 13809–13817, 2008.
[75] Y. N. Zhang, Y. Zhao, and R. Q. Lv, “A review for optical sensors based on photonic crystal cavities,” *Sensors Actuators, A Phys.*, vol. 233, pp. 374–389, 2015.
[76] L. Huang, H. Tian, J. Zhou, Q. Liu, P. Zhang, and Y. Ji, “Label-free optical sensor by designing a high-Q photonic crystal ring–slot structure,” *Opt. Commun.*, vol. 335, pp. 73–77, 2015.
[77] A. Di Falco, L. O’faolain, and T. F. Krauss, “Chemical sensing in slotted photonic crystal heterostructure cavities,” *Appl. Phys. Lett.*, vol. 94, no. 6, p. 63503, 2009.
[78] S. Hamed Mirsadeghi, E. Schelew, and J. F. Young, “Photonic crystal slot-microcavity circuit implemented in silicon-on-insulator: High Q operation in solvent without undercutting,” *Appl. Phys. Lett.*, vol. 102, no. 13, p. 131115, 2013.
[79] C. Caër, S. F. Serna-Otálvaro, W. Zhang, X. Le Roux, and E. Cassan, “Liquid sensor based on high-Q slot photonic crystal cavity in silicon-on-insulator configuration,” *Opt. Lett.*, vol. 39, no. 20, pp. 5792–5794, 2014.
[80] P. Bing, J. Yao, Y. Lu, and Z. Li, “A surface-plasmon-resonance sensor based on photonic-crystal-fiber with large size microfluidic channels,” *Opt. Appl*, vol. 42, no. 3, pp. 493–501, 2012.
[81] B. Li, L. Jiang, S. Wang, Q. C. M. Wang, and J. Yang, “A new Mach-Zehnder interferometer in a thinned-cladding fiber fabricated by electric arc for high sensitivity refractive index sensing,” *Opt. Lasers Eng.*, vol. 50, no. 6, pp. 829–832, 2012.
[82] G. Quero, A. Crescitelli, D. Paladino, M. Consales, A. Buosciolo, M. Giordano, A. Cutolo, and A. Cusano, “Evanescent wave long-period fiber grating within D-shaped optical fibers for high sensitivity refractive index detection,” *Sensors Actuators B Chem.*, vol. 152, no. 2, pp. 196–205, 2011.
[83] R. Gao, Y. Jiang, W. Ding, Z. Wang, and D. Liu, “Filmed extrinsic Fabry–Perot interferometric sensors for the measurement of arbitrary refractive index of liquid,” *Sensors Actuators B Chem.*, vol. 177, pp. 924–928, 2013.
[84] S. Romano, S. Torino, G. Coppola, S. Cabrini, and V. Mocella, “Optical sensors based on photonic crystal: A new route,” *Proc. SPIE - Int. Soc. Opt. Eng.*, vol. 10231, 2017.
[85] J. B. Jensen, L. H. Pedersen, P. E. Hoiby, L. B. Nielsen, T. P. Hansen, J. R. Folkenberg, J. Riishede, D. Noordegraaf, K. Nielsen, and A. Carlsen, “Photonic crystal fiber based evanescent-wave sensor for detection of biomolecules in aqueous solutions,” *Opt. Lett.*, vol. 29, no. 17, pp. 1974–1976, 2004.
[86] Y. L. Hoo, W. Jin, C. Shi, H. L. Ho, D. N. Wang, and S. C. Ruan, “Design and modeling of a photonic crystal fiber gas sensor,” *Appl. Opt.*, vol. 42, no. 18, pp. 3509–3515, 2003.
[87] A. Yariv and P. Yeh, *Optical waves in crystals*, vol. 5. Wiley New York, 1984.
[88] S. Chakravarty, J. Topol’ančik, P. Bhattacharya, S. Chakrabarti, Y. Kang, and M. E. Meyerhoff, “Ion detection with photonic crystal microcavities,” *Opt. Lett.*, vol. 30, no. 19, pp. 2578–2580, 2005.
[89] W.-C. Lai, S. Chakravarty, Y. Zou, and R. T. Chen, “Silicon nano-membrane based

photonic crystal microcavities for high sensitivity bio-sensing," *Opt. Lett.*, vol. 37, no. 7, pp. 1208–1210, 2012.
[90] M. Lee and P. M. Fauchet, "Two-dimensional silicon photonic crystal based biosensing platform for protein detection," *Opt. Express*, vol. 15, no. 8, pp. 4530–4535, 2007.
[91] M. R. Lee and P. M. Fauchet, "Nanoscale microcavity sensor for single particle detection," *Opt. Lett.*, vol. 32, no. 22, pp. 3284–3286, 2007.
[92] S. Zlatanovic, L. W. Mirkarimi, M. M. Sigalas, M. A. Bynum, E. Chow, K. M. Robotti, G. W. Burr, S. Esener, and A. Grot, "Photonic crystal microcavity sensor for ultracompact monitoring of reaction kinetics and protein concentration," *Sensors Actuators B Chem.*, vol. 141, no. 1, pp. 13–19, 2009.
[93] F. Hsiao and C. Lee, "Computational study of photonic crystals nano-ring resonator for biochemical sensing," *IEEE Sens. J.*, vol. 10, no. 7, pp. 1185–1191, 2010.
[94] F.-L. Hsiao and C. Lee, "Nanophotonic biosensors using hexagonal nanoring resonators: computational study," *J. Micro/Nanolithography, MEMS, MOEMS*, vol. 10, no. 1, p. 13001, 2011.
[95] F. Villa, L. E. Regalado, F. Ramos-Mendieta, J. Gaspar-Armenta, and T. Lopez-Ríos, "Photonic crystal sensor based on surface waves for thin-film characterization," *Opt. Lett.*, vol. 27, no. 8, pp. 646–648, 2002.
[96] M. Duneau, F. Delyon, and M. Audier, "Holographic method for a direct growth of three-dimensional photonic crystals by chemical vapor deposition," *J. Appl. Phys.*, vol. 96, no. 5, pp. 2428–2436, 2004.
[97] D. N. Sharp, A. J. Turberfield, and R. G. Denning, "Holographic photonic crystals with diamond symmetry," *Phys. Rev. B*, vol. 68, no. 20, p. 205102, 2003.
[98] T. Senn, J. Bischoff, N. Nüsse, M. Schoengen, and B. Löchel, "Fabrication of photonic crystals for applications in the visible range by nanoimprint lithography," *Photonics Nanostructures-Fundamentals Appl.*, vol. 9, no. 3, pp. 248–254, 2011.
[99] B. Troia, A. Paolicelli, F. De Leonardis, and V. M. N. Passaro, "Photonic crystals for optical sensing: A review," in *Advances in Photonic Crystals*, InTech, 2013.
[100] M. Fu, J. Liao, Z. Shao, M. Marko, Y. Zhang, X. Wang, and X. Li, "Finely engineered slow light photonic crystal waveguides for efficient wideband wavelength-independent higher-order temporal solitons," *Appl. Opt.*, vol. 55, no. 14, pp. 3740–3745, 2016.
[101] H. Sharifi, S. M. Hamidi, and K. Navi, "A new design procedure for all-optical photonic crystal logic gates and functions based on threshold logic," *Opt. Commun.*, vol. 370, pp. 231–238, 2016.
[102] M. Djavid and M. S. Abrishamian, "Multi-channel drop filters using photonic crystal ring resonators," *Optik - International Journal for Light and Electron Optics*, vol. 123, no. 2. Elsevier GmbH., pp. 167–170, 2012.
[103] S. Robinson and R. Nakkeeran, "Two dimensional Photonic Crystal Ring Resonator based Add Drop Filter for CWDM systems," *Opt. - Int. J. Light Electron Opt.*, vol. 124, no. 18, pp. 3430–3435, 2013.
[104] A. Rostami, F. Nazari, H. A. Banaei, and A. Bahrami, "A novel proposal for DWDM demultiplexer design using modified-T photonic crystal structure," *Photonics Nanostructures - Fundam. Appl.*, vol. 8, no. 1, pp. 14–22, 2010.
[105] M. Youcef Mahmoud, G. Bassou, and A. Taalbi, "A new optical add–drop filter based on two-dimensional photonic crystal ring resonator," *Opt. - Int. J. Light Electron Opt.*, vol. 124, no. 17, pp. 2864–2867, 2013.

[106] H. Alipour-Banaei and F. Mehdizadeh, "Significant role of photonic crystal resonant cavities in WDM and DWDM communication tunable filters," *Opt. - Int. J. Light Electron Opt.*, vol. 124, no. 17, pp. 2639–2644, Sep. 2013.
[107] M. Djavid, F. Monifi, a. Ghaffari, and M. S. Abrishamian, "Heterostructure wavelength division demultiplexers using photonic crystal ring resonators," *Opt. Commun.*, vol. 281, no. 15–16, pp. 4028–4032, Aug. 2008.
[108] F. Mehdizadeh, H. Alipour-Banaei, and S. Serajmohammadi, "Channel-drop filter based on a photonic crystal ring resonator," *J. Opt.*, vol. 15, no. 7, p. 075401, Jul. 2013.
[109] H. Alipour-Banaei, F. Mehdizadeh, and M. Hassangholizadeh-Kashtiban, "A new proposal for PCRR-based channel drop filter using elliptical rings," *Phys. E Low-dimensional Syst. Nanostructures*, vol. 56, pp. 211–215, Feb. 2014.
[110] C.-W. Kuo, C.-F. Chang, M.-H. Chen, S.-Y. Chen, and Y.-D. Wu, "A new approach of planar multi-channel wavelength division multiplexing system using asymmetric super-cell photonic crystal structures," *Opt. Express*, vol. 15, pp. 198–206, 2007.
[111] Y. Liu and H. W. M. Salemink, "Sensitive All-Optical Channel-Drop Sensor in Photonic Crystals," *J. Light. Technol.*, vol. 33, no. 17, pp. 3672–3678, 2015.
[112] Y. Liu and H. W. M. Salemink, "Photonic crystal-based all-optical on-chip sensor," *Opt. Express*, vol. 20, no. 18, p. 19912, Aug. 2012.
[113] U. P. Dharanipathy, M. Minkov, M. Tonin, V. Savona, and R. Houdré, "High-Q silicon photonic crystal cavity for enhanced optical nonlinearities," *Appl. Phys. Lett.*, vol. 105, no. 10, p. 101101, 2014.
[114] N. V. Triviño, M. Minkov, G. Urbinati, M. Galli, J.-F. Carlin, R. Butté, V. Savona, and N. Grandjean, "Gallium nitride L3 photonic crystal cavities with an average quality factor of 16 900 in the near infrared," *Appl. Phys. Lett.*, vol. 105, no. 23, p. 231119, 2014.
[115] M. Minkov and V. Savona, "Automated optimization of photonic crystal slab cavities.," *Sci. Rep.*, vol. 4, p. 5124, 2014.
[116] M. Djavid, S. A. Mirtaheri, and M. S. Abrishamian, "Photonic crystal notch-filter design using particle swarm optimization theory and finite-difference time-domain analysis," *J. Opt. Soc. Am. B*, vol. 26, no. 4, pp. 849–853, 2009.
[117] L. Jiang, H. Wu, W. Jia, and X. Li, "Optimization of low-loss and wide-band sharp photonic crystal waveguide bends using the genetic algorithm," *Opt. - Int. J. Light Electron Opt.*, vol. 124, no. 14, pp. 1721–1725, Aug. 2013.
[118] S. M. Mirjalili, S. Mirjalili, and S. Z. Mirjalili, "How to design photonic crystal LEDs with artificial intelligence techniques," *Electron. Lett.*, vol. 51, no. 18, pp. 1437–1439, 2015.
[119] S. M. Mirjalili and S. Z. Mirjalili, "Asymmetric Oval-Shaped-Hole Photonic Crystal Waveguide design by Artificial Intelligence Optimizers," *IEEE J. Sel. Top. Quantum Electron.*, vol. 22, no. 2, p. 4900407, 2016.
[120] S. M. Mirjalili and S. Z. Mirjalili, "Full Optimizer for Designing Photonic Crystal Waveguides: IMoMIR framework," *IEEE Photonics Technol. Lett.*, vol. 27, no. 16, pp. 1776–1779, 2015.
[121] S. M. Mirjalili, "SoMIR framework for designing high-NDBP photonic crystal waveguides," *Appl. Opt.*, vol. 53, no. 18, pp. 3945–3953, 2014.
[122] S. M. Mirjalili, S. Mirjalili, and A. Lewis, "A Novel Multi-Objective Optimization Framework for Designing Photonic Crystal Waveguides," *Photonics Technol. Lett. IEEE*, vol. 26, no. 2, pp. 146–149, 2014.

[123] S. Saremi, S. M. Mirjalili, and S. Mirjalili, "Unit Cell Topology Optimization of Line Defect Photonic Crystal Waveguide," *Procedia Technol.*, vol. 12, pp. 174–179, Jan. 2014.
[124] S. M. Mirjalili, K. Abedi, and S. Mirjalili, "Optical buffer performance enhancement using Particle Swarm Optimization in Ring-Shape-Hole Photonic Crystal Waveguide," *Opt. - Int. J. Light Electron Opt.*, vol. 124, no. 23, pp. 5989–5993, Dec. 2013.
[125] S. M. Mirjalili, K. Abedi, and S. Mirjalili, "Light property and optical buffer performance enhancement using particle swarm optimization in oblique ring-shape-hole photonic crystal waveguide," in *Photonics Global Conference (PGC)*, 2012, pp. 1–4.
[126] S. M. Mirjalili, S. Z. Mirjalili, and S. Mirjalili, "Multi-Objective Vs. Single-Objective Optimization Frameworks for Designing Photonic Crystal Filters," *Appl. Opt.*, vol. 56, no. 36, p. In press, 2017.
[127] S. M. Mirjalili and S. Z. Mirjalili, "Single-objective optimization framework for designing photonic crystal filters," *Neural Comput. Appl.*, vol. 28, no. 6, pp. 1463–1469, 2017.
[128] S. Guo and S. Albin, "Simple plane wave implementation for photonic crystal calculations," *Opt. Express*, vol. 11, no. 2, pp. 167–175, Jan. 2003.
[129] A. Säynätjoki, M. Mulot, J. Ahopelto, and H. Lipsanen, "Dispersion engineering of photonic crystal waveguides with ring-shaped holes," *Opt. Express*, vol. 15, no. 13, pp. 8323–8328, Jun. 2007.
[130] C. A. Coello Coello and M. S. Lechuga, "MOPSO: A proposal for multiple objective particle swarm optimization," in *Evolutionary Computation, 2002. CEC'02. Proceedings of the 2002 Congress on*, 2002, vol. 2, pp. 1051–1056.
[131] S. Mirjalili, S. M. Mirjalili, and A. Hatamlou, "Multi-Verse Optimizer: a nature-inspired algorithm for global optimization," *Neural Comput. Appl.*, vol. 27, no. 2, pp. 495–513, 2016.
[132] S. Mirjalili, A. H. Gandomi, S. Z. Mirjalili, S. Saremi, H. Faris, and S. M. Mirjalili, "Salp Swarm Algorithm: A bio-inspired optimizer for engineering design problems," *Adv. Eng. Softw.*, p. In press, 2017.
[133] S. Mirjalili, S. Saremi, S. M. Mirjalili, and L. dos S. Coelho, "Multi-objective grey wolf optimizer: A novel algorithm for multi-criterion optimization," *Expert Syst. Appl.*, vol. 47, pp. 106–119, Apr. 2016.
[134] S. Mirjalili, S. M. Mirjalili, and A. Lewis, "Grey Wolf Optimizer," *Adv. Eng. Softw.*, vol. 69, pp. 46–61, Mar. 2014.
[135] S. Saremi, S. Z. Mirjalili, and S. M. Mirjalili, "Evolutionary population dynamics and grey wolf optimizer," *Neural Comput. Appl.*, vol. 26, no. 5, pp. 1257–1263, 2015.
[136] H. Faris, I. Aljarah, M. A. Al-Betar, and S. Mirjalili, "Grey wolf optimizer: a review of recent variants and applications," *Neural Comput. Appl.*, pp. 1–23, 2017.
[137] S. M. Mirjalili, S. Mirjalili, A. Lewis, and K. Abedi, "A tri-objective Particle Swarm Optimizer for designing line defect Photonic Crystal Waveguides," *Photonics Nanostructures - Fundam. Appl.*, vol. 12, no. 2, pp. 152–163, Apr. 2014.
[138] J. Kennedy and R. Eberhart, "Particle swarm optimization," *Proc. ICNN'95 - Int. Conf. Neural Networks*, vol. 4, pp. 1942–1948, 1995.
[139] R. Eberhart and J. Kennedy, "A new optimizer using particle swarm theory," *MHS'95. Proc. Sixth Int. Symp. Micro Mach. Hum. Sci.*, pp. 39–43, 1995.
[140] L. D. Davis and M. Mitchell, "Handbook of Genetic Algorithms," *VAN NOSTRAND REINHOLD*, vol. 15, no. 1, pp. 4–6, 1991.
[141] M. Notomi, T. Tanabe, A. Shinya, E. Kuramochi, and H. Taniyama, "On-Chip All-Optical

Switching and Memory by Silicon Photonic Crystal Nanocavities," *Advances in Optical Technologies*, vol. 2008. pp. 1–10, 2008.

[142] L. O'Faolain, T. P. White, D. O'Brien, X. Yuan, M. D. Settle, and T. F. Krauss, "Dependence of extrinsic loss on group velocity in photonic crystal waveguides.," *Opt. Express*, vol. 15, no. 20, pp. 13129–13138, 2007.

[143] M. J. Safdari, S. M. Mirjalili, P. Bianucci, and X. Zhang, "Multi-objective optimization framework for designing photonic crystal sensors," *Appl. Opt.*, vol. 57, no. 8, p. 1950, 2018.